IEEE Access
Multidisciplinary | Rapid Review | Open Access Journal

Received November 20, 2020, accepted December 3, 2020, date of publication December 8, 2020,
date of current version December 21, 2020.

Digital Object Identifier 10.1109/ACCESS.2020.3043254

Optimization Methods to Reduce Capacitor Stress in Modular Multilevel Converters

NIKOLA PETRANOVIC[1], (Member, IEEE), ANTONIO CANTONI[1], (Life Fellow, IEEE), CHRISTOPHER D. TOWNSEND[1], (Member, IEEE), AND GEORGIOS KONSTANTINOU[2], (Senior Member, IEEE)

[1]Department of Electrical, Electronic and Computer Engineering, The University of Western Australia, Crawley, WA 6009, Australia
[2]School of Electrical Engineering and Telecommunications, University of New South Wales, Kensington, NSW 2052, Australia

Corresponding author: Nikola Petranovic (nikola.petranovic@research.uwa.edu.au)

The work of Nikola Petranovic was supported in part by a Samaha Research Scholarship, and in part by an Australian Government Research Training Program Scholarship at The University of Western Australia.

ABSTRACT Modular multilevel converters consist of many capacitor half-bridge or full-bridge converter cells. Stresses on the capacitors result from peak capacitor voltage, capacitor voltage ripple and current ripple. Three new tractable convex optimisation problems are presented that reduce peak capacitor voltage and limit rms arm current using injected zero-sequence voltages, circulating currents and selecting the initial stored capacitor energy. These optimisation problems are compared to assess their performance in terms of key indicators which include factors related to capacitor stress, capacitor and semiconductor ratings, and power loss: peak capacitor voltage, capacitor voltage ripple, capacitor current ripple, average and rms arm current. The optimisation methods permit designers to understand the trade-offs in achieving the limits imposed by device specifications and power losses.

INDEX TERMS Design optimisation, equivalent circuits, modelling, modular multilevel converters.

I. INTRODUCTION

A high efficiency converter with medium and high power applications is the modular multilevel converter (MMC) [1]–[4]. A circuit schematic of a three-phase MMC is shown in Fig. 1. Each MMC leg (*a,b,c*) contains two arms (upper *u* and lower *l*), each of which consists of serially connected *submodules* (SMs) which are full-bridge capacitor cells (or alternatively half-bridge cells [5]).

An important consideration in the design of MMCs is to limit the stress on the components. Current ratings of semiconductors and capacitors require limits on the maximum arm current. Power losses and thermal stresses on semiconductors are related to rms currents [6], [7]. The stress on capacitors depend upon the peak capacitor voltage [8], [9]. Selection of semiconductor voltage specification is based upon the maximum peak capacitor voltage [10]. Other stresses on capacitors are caused by ripple voltage and ripple current [9], [11].

To decrease stress on capacitors, papers in the literature proposed methods that determine the zero-sequence voltages and/or circulating currents to reduce peak-to-peak voltage ripple [12]–[21] or peak capacitor voltage [22]. Brief summaries of some of these papers are given below:

Exhaustive search methods exist that minimise peak-to-peak capacitor voltage ripple using circulating currents [12], [13]. The disadvantages of exhaustive search techniques relative to optimisation-based solvers are time-inefficiency and the solution's dependence on quantisation of optimisation parameters. In [12], the magnitude and phase angle of a second-order and a fourth-order circulating current harmonic are exhaustively sought to find optimal solutions for three optimisation problems: the minimisation of capacitor voltage ripple; the minimisation of a weighted sum of capacitor voltage ripple and rms current, and; the minimisation of capacitor voltage ripple subject to a constraint on rms current. The authors of [13] present an exhaustive search of the same circulating current harmonic parameters as those considered in [12]. The method presented in [13] also minimises capacitor voltage ripple, however the authors utilise a different model for capacitor voltage that is proposed in [23]. The technique studied in [13] was designed to overcome the drawbacks of another method to reduce capacitor voltage ripple, shown in [14], in which an approximate expression for capacitor voltage ripple is minimised using circulating currents. Neither

The associate editor coordinating the review of this manuscript and approving it for publication was Giambattista Gruosso.

[13] or [14] include any other component or system stress related constraints, such as constraints on peak capacitor voltage.

The authors of [22] show a technique that is used to determine only the second order circulating current that decreases peak capacitor voltage. Namely, an exhaustive approach is used to find the phase angle and magnitude of the circulating current such that the capacitor voltage has a zero first-order derivative at a certain point in time. This method is used as a means to avoid excessive capacitor voltages that stress the MMC components. However, no constraints are considered to enforce limits on power loss and stress on MMC components.

The authors of [15], [16] suggest analytical methods that determine circulating currents, under conditions in which a zero-sequence voltage is injected, that remove low-frequency capacitor energy fluctuation terms. This method is utilised as an approach to reduce capacitor voltage ripple relative to the case in which no harmonic voltages and currents are injected. However, there are no constraints imposed on the selection of circulating currents that limit the increases in peak or rms arm current.

The authors of [17] proposed an optimisation problem that minimises the rms value of circulating currents subject to a low-frequency capacitor voltage term equal to zero. This equality constraint is proposed as an approach to reduce capacitor voltage ripple. Again, the method in this paper does not include other constraints that set upper bounds on quantities that relate to component stress, such as peak capacitor voltage, peak arm voltages or peak arm currents.

The authors of [18], [19] consider optimisation problems that minimise objective functions that contain a linear combination of variables that influence capacitor stress and MMC power losses. A two-step linear programming method is considered in [18] that uses auxiliary optimisation parameters that provide upper and lower bounds to stored capacitor energy, an upper bound on average current, and upper bounds on harmonic zero-sequence voltage magnitudes. A linear combination of these auxiliary variables form the objective functions considered in [18] for each linear program step. The primary purpose of the technique studied in [18] is to reduce capacitor voltage ripple subject to constraints on peak arm voltage, peak arm current and average arm current. However, there was no method to minimise the peak capacitor voltage, which is a key metric in determining overall capacitor and semiconductor stress. The Matlab function *linprog*, together with the *interior-point-legacy* algorithm [24], [25] are used to solve each optimisation step. A nonlinear objective function that consists of a weighted-sum of capacitor energy ripple, rms current and rate of change of arm voltages and currents is considered in [19], which was solved using a nonlinear Matlab solver function *fmincon*.

In this paper, new and tractable convex optimisation problems are proposed that allow designers to understand the trade-offs in achieving the limits imposed by device specifications and power losses, and thus permit informed decisions in the design phase. Well-established and reliable optimisation

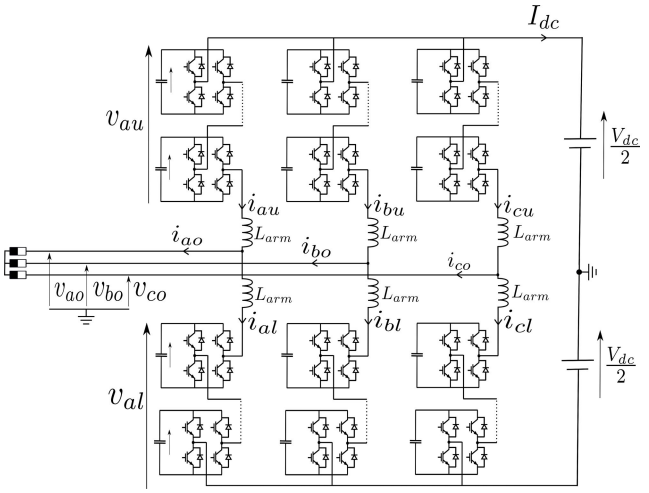

FIGURE 1. Circuit schematic of a modular multilevel converter with a balanced three-phase load.

algorithms can be used to solve the problems presented in this paper. The parameters over which the optimisation problems are solved include zero-sequence voltages, circulating currents and initial capacitor energy. In the proposed optimisation problems, constraints are included that are necessary and sufficient to impose upper limits on peak arm currents, peak rms arm currents and peak arm voltages. These constraints can be tightened and loosened to explore the design space and the trade-offs in terms of key performance indicators: peak capacitor voltage, peak-to-peak capacitor ripple voltages and currents, rms and average arm current. These performance indicators are selected because they are important contributors to capacitor stress [8], [9], [11] and MMC power losses [7].

The key contributions of this paper are: 1. A detailed formulation of a simplified MMC model with all assumption clearly described. 2. Three new and tractable two-step convex optimisation problems that reduce peak capacitor voltage using injected zero-sequence voltages, circulating current and initial capacitor energy. 3. The introduction of an optimisation constraint which imposes an upper limit on rms arm current. 4. The solutions to each of the three two-step optimisation problems are compared in terms of key performance indicators related to capacitor stress and power losses to illustrate, for the first time, the trade-offs achievable with optimised MMC designs.

The paper is structured as follows. The MMC model is derived in Section II. Novel two-step convex optimisation methods are described in Section III. The methods for solving the convex optimisation problems and their results are considered in Section IV. Summary remarks are given in Section V.

II. MODELLING

In this section, the MMC arm voltages, current and capacitor energy are modelled in terms of the nominal (operational) condition parameters, injected zero-sequence voltage

and circulating currents parameters, and MMC components parameters. Tellegen's theorem is used to derive a model for the stored capacitor energy in an arm as a function of the arm voltage and arm current. Similar stored capacitor energy relationships have been reported in [9], [12], [18], [20], [22], however alternative assumptions are used and it is not clear how these models are related to the one proposed in this paper. Experimental validation of the model is presented in Section III-C. The optimisation criteria and constraints in the optimisation problems, which are introduced in Section III, are defined in terms of this model's voltages, currents and energies.

A. ARM VOLTAGES AND CURRENTS

With reference to Fig. 1, let $v_{pq}(t)$ and $i_{pq}(t)$ denote voltages and currents in an arm, where $p \in \{a, b, c\}$, and $q \in \{u, l\}$. The voltages and currents in the upper and lower arms of the MMC, $v_{pu}(t)$, $i_{pu}(t)$, $v_{pl}(t)$ and $i_{pl}(t)$, are defined in (1)-(4).

$$\begin{aligned} &v_{pu}(t) \\ &\triangleq \underbrace{\frac{V_{dc}}{2} - V_{1g}\cos(\omega_0(t-T_p)) - V_{1h}\sin(\omega_0(t-T_p))}_{v_{\mathrm{N}pu}(t)} \\ &\quad \underbrace{- \sum_{m\in\mathcal{V}} \left[V_{mg}\cos(m\omega_0(t-T_p)) + V_{mh}\sin(m\omega_0(t-T_p))\right]}_{v_{\mathrm{IV}pu}(t)} \end{aligned} \tag{1}$$

$$\begin{aligned} &i_{pu}(t) \\ &\triangleq \underbrace{-\frac{I_{dc}}{3} + I_{1g}\cos(\omega_0(t-T_p)) + I_{1h}\sin(\omega_0(t-T_p))}_{i_{\mathrm{N}pu}(t)} \\ &\quad \underbrace{- \sum_{m\in\mathcal{I}} \left[I_{mg}\cos(m\omega_0(t-T_p)) + I_{mh}\sin(m\omega_0(t-T_p))\right]}_{i_{\mathrm{CC}pu}(t)} \end{aligned} \tag{2}$$

$$\begin{aligned} &v_{pl}(t) \\ &\triangleq \underbrace{\frac{V_{dc}}{2} + V_{1g}\cos(\omega_0(t-T_p)) + V_{1h}\sin(\omega_0(t-T_p))}_{v_{\mathrm{N}pl}(t)} \\ &\quad \underbrace{+ \sum_{m\in\mathcal{V}} \left[V_{mg}\cos(m\omega_0(t-T_p)) + V_{mh}\sin(m\omega_0(t-T_p))\right]}_{v_{\mathrm{IV}pl}(t)} \end{aligned} \tag{3}$$

$$\begin{aligned} &i_{pl}(t) \\ &\triangleq \underbrace{-\frac{I_{dc}}{3} - I_{1g}\cos(\omega_0(t-T_p)) - I_{1h}\sin(\omega_0(t-T_p))}_{i_{\mathrm{N}pl}(t)} \\ &\quad \underbrace{- \sum_{m\in\mathcal{I}} \left[I_{mg}\cos(m\omega_0(t-T_p)) + I_{mh}\sin(m\omega_0(t-T_p))\right]}_{i_{\mathrm{CC}pl}(t)} \end{aligned} \tag{4}$$

where ω_0 is the fundamental frequency, $T_0 = 2\pi/\omega_0$ and

$$T_p = \begin{cases} 0, & p = a \\ T_0/3, & p = b \\ 2T_0/3, & p = c \end{cases} \tag{5}$$

The arm voltages and currents have been formulated generically to include nominal voltage $v_{\mathrm{N}pq}(t)$ and current $i_{\mathrm{N}pq}(t)$, injected voltages, $v_{\mathrm{IV}pq}(t)$, and circulating currents, $i_{\mathrm{CC}pq}(t)$; which can be created in an MMC [12]–[21], [26], [27]. The T_0-periodic arm voltages and currents are formulated to be three-phase time offset by $T_0/3$. In (1)-(4) the harmonics due to PWM switching in the SMs are assumed to be negligible and the arm inductances are assumed to be small so that the arm voltages required to create the arm currents are insignificant. In the general case the harmonics injected in arm voltages and currents in (1)-(4) are assumed to be harmonics of the fundamental ω_0 up to some maximum N_H as defined by the sets $\mathcal{V}$ and $\mathcal{I}$.

$$\mathcal{V} \triangleq \{2, \ldots, N_H\} \tag{6}$$

$$\mathcal{I} \triangleq \{2, \ldots, N_H\} \tag{7}$$

The arm voltage and currents are re-written in vector form in (8)-(11), where $\mathbf{f}_p(t)$, $\mathbf{x}_v$ and $\mathbf{x}_i$ are defined in the Appendix A.

$$v_{pu}(t, \mathbf{x}_v) = v_{\mathrm{N}pu}(t) - \mathbf{f}_p^T(t)\mathbf{x}_v \tag{8}$$

$$i_{pu}(t, \mathbf{x}_i) = i_{\mathrm{N}pu}(t) - \mathbf{f}_p^T(t)\mathbf{x}_i \tag{9}$$

$$v_{pl}(t, \mathbf{x}_v) = v_{\mathrm{N}pl}(t) + \mathbf{f}_p^T(t)\mathbf{x}_v \tag{10}$$

$$i_{pl}(t, \mathbf{x}_i) = i_{\mathrm{N}pl}(t) - \mathbf{f}_p^T(t)\mathbf{x}_i \tag{11}$$

B. STORED CAPACITOR ENERGY

The circuit in Fig. 2 shows the serially connected submodules in any arm pq. In Fig. 2, the rest of the MMC circuit is represented by the one-port element characterised by the relationship of arm voltage to arm current, $v_{pq}(t, \mathbf{x}_v)$ and $i_{pq}(t, \mathbf{x}_i)$ as defined in (8) to (11).

$v_{Dpq_{j,k}}(t)$ and $i_{Dpq_{j,k}}(t)$ represent the voltage and current at k^{th} switch on the j^{th} submodule where $k = 1, \ldots, 4$ and $j = 1, \ldots, J$. C_{SM_j}, $v_{Cpq_j}(t)$ and $i_{Cpq_j}(t)$ represents the capacitance, voltage and current of the j^{th} submodule capacitor. Using Tellegen's theorem [28] for the circuit in Fig. 2:

$$\begin{aligned} &\sum_{j=1}^{J}\sum_{k=1}^{4}\left[v_{Dpq_{j,k}}(t)i_{Dpq_{j,k}}(t)\right] - v_{pq}(t, \mathbf{x}_v)i_{pq}(t, \mathbf{x}_i) \\ &\qquad + \sum_{j=1}^{J} v_{Cpq_j}(t)i_{Cpq_j}(t) = 0 \end{aligned} \tag{12}$$

Assuming ideal lossless switches, then the first term in (12) is zero. Under this assumption, and considering the definite

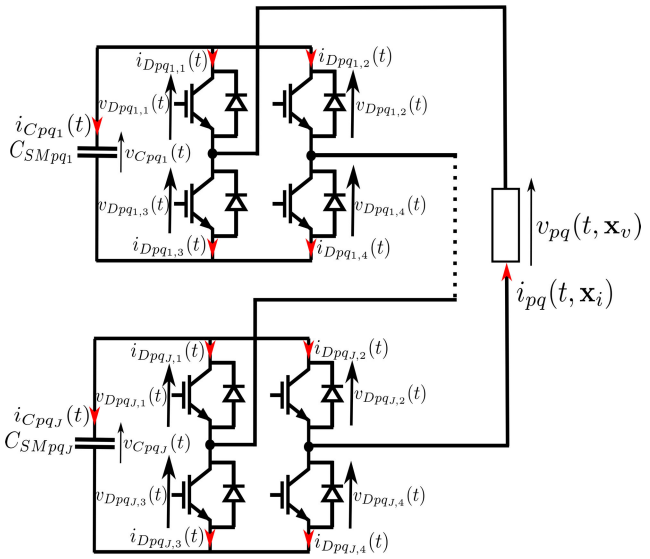

FIGURE 2. Equivalent MMC circuit illustrating an arm connected to a one-port element which represents the rest of the MMC circuit.

integral of (12), it follows that:

$$-\int_{t_0+T_{pq}}^{t+T_{pq}} v_{pq}(\tau, \mathbf{x}_v) i_{pq}(\tau, \mathbf{x}_i) d\tau + \sum_{j=1}^{J} \int_{t_0+T_{pq}}^{t+T_{pq}} v_{Cpq_j}(\tau) i_{Cpq_j}(\tau) d\tau = 0 \quad (13)$$

where

$$T_{pq} \triangleq T_p + T_q \quad (14)$$

$$T_q = \begin{cases} 0, & q = u \\ \alpha, & q = l \end{cases} \quad (15)$$

The parameter α is introduced to allow for a time shift that exists, for the cases of interest in the paper, between the upper and lower arm voltage and current functions in the same phase, as defined in (16).

$$\begin{aligned} v_{pl}(t, \mathbf{x}_v) &= v_{pu}(t - \alpha, \mathbf{x}_v), \quad \forall p \\ i_{pl}(t, \mathbf{x}_v) &= i_{pu}(t - \alpha, \mathbf{x}_i), \quad \forall p \end{aligned} \quad (16)$$

The value of α is determined in Section III-B7 for a special set of $\mathcal{V}$ and $\mathcal{I}$ that are of interest in this paper.

From (13) and the voltage-current relationship in a capacitor, it follows that:

$$\sum_{j=1}^{J} \left[\frac{C_{SMpq_j}}{2} \left(v_{Cpq_j}^2(t + T_{pq}) - v_{Cpq_j}^2(t_0 + T_{pq}) \right) \right] = \int_{t_0+T_{pq}}^{t+T_{pq}} v_{pq}(\tau, \mathbf{x}_v) i_{pq}(\tau, \mathbf{x}_i) d\tau \quad (17)$$

It is assumed that there are balanced capacitor voltages and equal submodule capacitor currents in an arm, i.e.

$$v_{Cpq}(t) = v_{Cpq_j}(t), \; i_{Cpq}(t) = i_{Cpq_j}(t), \quad j = 1, \ldots, J \quad (18)$$

Control strategies for achieving the balance described in (18) have been proposed in the literature [23].

Given every SM capacitor has the same capacitance, C_{SM}, the subscript j is dropped from (17) to obtain:

$$\int_{t_0+T_{pq}}^{t+T_{pq}} v_{pq}(\tau, \mathbf{x}_v) i_{pq}(\tau, \mathbf{x}_i) d\tau = \frac{JC_{SM}}{2} \left(v_{Cpq}^2(t + T_{pq}) - v_{Cpq}^2(t_0 + T_{pq}) \right) \quad (19)$$

Consider the definitions in (20)-(22).

$$C_{\text{eff}} \triangleq \frac{C_{SM}}{J} \quad (20)$$

$$e_{Cpq}(t + T_{pq}) \triangleq \frac{C_{\text{eff}}}{2} (J v_{Cpq}(t + T_{pq}))^2 \quad (21)$$

$$x_{e_{C0}pq}(t_0 + T_{pq}) \triangleq \frac{C_{\text{eff}}}{2} (J v_{Cpq}(t_0 + T_{pq}))^2 \quad (22)$$

Equation (19) is then re-written in terms of the variables C_{eff}, $e_{Cpq}(t)$ and $x_{e_{C0}pq}$ in (23).

$$e_{Cpq}(t + T_{pq}) = \int_{t_0+T_{pq}}^{t+T_{pq}} v_{pq}(\tau, \mathbf{x}_v) i_{pq}(\tau, \mathbf{x}_i) d\tau + x_{e_{C0}pq}(t_0 + T_{pq}) \quad (23)$$

The time-average, defined in (24), of the function $e_{Cpq}(t + T_{pq})$ is assumed to be equal in all the arms. This assumption is stated in (25). An experimental method to enforce (25) is described in [26].

$$\underset{t}{\text{ave}}\,(\cdot) = \frac{1}{T_0} \int_{t_0}^{t_0+T_0} (\cdot)\, dt \quad (24)$$

$$\underset{t}{\text{ave}} \left[e_{Cpq}(t + T_{pq}) \right] = \underset{t}{\text{ave}} \left[e_{Cau}(t) \right], \quad \forall p, q \quad (25)$$

Using the arm voltage and current relationships defined in (1)-(4) and (16), it can be shown that (25) implies (26). The derivation is detailed in Appendix C.

$$x_{e_{C0}pq}(t_0 + T_{pq}) = x_{e_{C0}au}(t_0) \quad (26)$$

It follows from (26), that the $e_{Cpq}(t + T_{pq})$ in the MMC arms are time-offset in the same manner as the voltages and currents as defined in (1)-(4), (16), as described in (27). The derivation of (27) is detailed in Appendix C.

$$e_{Cpq}(t + T_{pq}) = e_{Cau}(t) \Leftrightarrow e_{Cpq}(t) = e_{Cau}(t - T_{pq}) \quad (27)$$

An interpretation of (27) is: the behaviour of $e_{Cpq}(t + T_{pq})$ for *all* pq is known if $e_{Cpq}(t + T_{pq})$ for *any* pq is known.

As explained in Section III-B7, for a special subset of voltage and current harmonics, only one of the six arm's voltage, current and energy functions needs to be considered when solving the optimisation problems presented in this paper.

The upper arm of leg a, $p = a$ and $q = u$, is arbitrarily selected hereafter and for simplicity, the subscript au is dropped from the notation. Substituting $T_{pq} = T_{au} = 0$, (8) and (9) into (23), it can be shown that $e_C(t)$ in arm au can be

written as in (28). Furthermore, it is made explicit that $e_C(t)$ is a function of the $\mathbf{x}_v$, $\mathbf{x}_i$ and x_{eC0} in (28).

$$e_C(t, \mathbf{x}_v, \mathbf{x}_i, x_{eC0}) = x_{eC0} + \int_{t_0}^{t} v_{\mathrm{N}}(\tau) i_{\mathrm{N}}(\tau) d\tau - \mathbf{x}_v^T \boldsymbol{\varrho}_i(t) - \mathbf{x}_i^T \boldsymbol{\varrho}_v(t) + \mathbf{x}_v^T \mathbf{P}(t) \mathbf{x}_i \quad (28)$$

where $\boldsymbol{\varrho}_i(t)$, $\boldsymbol{\varrho}_v(t)$ and $\mathbf{P}(t)$ are defined in the Appendix A1.

III. OPTIMISATION PROBLEM FORMULATION

The optimisation problems proposed in this paper minimize the peak capacitor voltage subject to constraints, using the optimisation parameters that are controllable in the MMC: $\mathbf{x}_v$, $\mathbf{x}_i$ and x_{eC0}. The objective function, constraints and the proposed two-step optimisation problems are detailed in this section.

A. OBJECTIVE

Stresses on a capacitor arise from large peak voltages. In this paper, the objective function, $f_0(t, \mathbf{x}_v, \mathbf{x}_i, x_{eC0})$, of the optimisation problems is devised such that peak capacitor voltages are minimized, thereby decreasing stress on capacitors. Thus the objective function given by (29) is proposed.

$$f_0(t, \mathbf{x}_v, \mathbf{x}_i, x_{eC0}) \triangleq \max_t v_C(t, \mathbf{x}_v, \mathbf{x}_i, x_{eC0}) \quad (29)$$

For correct operation of the diode/switch assembly, the capacitor voltages need to be always positive, i.e. $v_C(t) \geq 0$, [29]. It follows from (29) and $v_C(t) \geq 0$ that the objective function defined by (30) is equivalent to that defined by (29).

$$\max_t e_C(t, \mathbf{x}_v, \mathbf{x}_i, x_{eC0}) \quad (30)$$

The objective function (30) avoids any issues associated with the square root operator which would arise in (29).

B. CONSTRAINTS

This section introduces the constraints that are utilized in the optimisation problems.

1) PEAK ARM CURRENT CONSTRAINT

The allowable peak arm current is dependent on the rating of the MMC IGBTs/semiconductors. Thus the magnitude of the current needs to be constrained below some specified maximum, as defined in (31).

$$|i(t, \mathbf{x}_i)| \leq I_{\mathrm{MAX}}, \quad \forall t \quad (31)$$

The two linear inequality constraints on the current in (32) are equivalent to the required constraint defined by (31).

$$i_{\mathrm{N}}(t) - \mathbf{f}^T(t)\mathbf{x}_i \leq I_{\mathrm{MAX}} \quad \forall t$$
$$-i_{\mathrm{N}}(t) + \mathbf{f}^T(t)\mathbf{x}_i \leq I_{\mathrm{MAX}} \quad \forall t \quad (32)$$

2) ROOT-MEAN-SQUARE CURRENT CONSTRAINT

Thermal limits of semiconductors and power loss considerations are addressed by imposing an upper bound on arm rms current. It can be shown that the rms current in an arm, $i_{rms}(\mathbf{x}_i)$ can be written in terms of nominal and injected circulating currents as given in (33).

$$i_{rms}(\mathbf{x}_i) = \sqrt{\frac{I_{dc}^2}{9} + \frac{I_{1g}^2}{2} + \frac{I_{1h}^2}{2} + \frac{1}{2}\mathbf{x}_i^T \mathbf{x}_i} \quad (33)$$

where

$$i_{rms}(\mathbf{x}_i) \triangleq \sqrt{\frac{1}{T_0}\int_{t_0}^{t_0+T_0} i^2(t, \mathbf{x}_i) dt} \quad (34)$$

It is clear from (33) that the injection of circulating currents increases the arm rms current relative to nominal conditions, that is

$$i_{rms}(\mathbf{x}_i = 0) \leq i_{rms}(\mathbf{x}_i) \quad (35)$$

Thus, as defined in (36) a parameter $I_{\mathrm{RMSF}} \geq 1$, is introduced to define an upper bound on the rms current. Note that the bound imposes a maximum relative to the nominal rms current.

$$i_{rms}(\mathbf{x}_i) \leq I_{\mathrm{RMSF}} i_{rms}(\mathbf{x}_i = 0) \quad (36)$$

Root-mean-square quantities are positive, and therefore deriving the root-mean-square current from the mean-square quantity involves a monotone transformation. Thus the constraint defined by (37) is equivalent to the constraint defined by (36).

$$\frac{I_{dc}^2}{9} + \frac{I_{1g}^2}{2} + \frac{I_{1h}^2}{2} + \frac{1}{2}\mathbf{x}_i^T \mathbf{x}_i \leq (I_{\mathrm{RMSF}} i_{rms}(\mathbf{x}_i = 0))^2 \quad (37)$$

Equation (37) is a direct way on placing an upper bound on the arm rms current as opposed to adding a term to the objective function [12], [19], which would require a decision on the weight to be placed on this term.

3) MINIMUM ARM VOLTAGE CONSTRAINT

For correct operation of MMC submodules implemented as unipolar (half-bridge) converter submodules, the arm voltages need to be greater than or equal to zero. Thus, the constraint (38) is proposed.

$$v(t, \mathbf{x}_v) \geq 0, \quad \forall t \quad (38)$$

It is not difficult to show that the more convenient form (39) is equivalent to (38).

$$v_{\mathrm{N}}(t) - \mathbf{f}^T(t)\mathbf{x}_v \geq 0, \quad \forall t \quad (39)$$

Note that bipolar (full-bridge) converter submodules can function as unipolar submodules, but the reverse is not true.

4) PEAK ARM VOLTAGE CONSTRAINT

Similar to peak currents, another constraint is introduced to place an upper limit on peak arm voltage as defined in (40).

$$|v(t, \mathbf{x}_v)| \leq V_{\mathrm{MAX}}, \quad \forall t \quad (40)$$

Given the inclusion of the constraint in (38), it is clear that (40) is equivalently achieved using (41).

$$v(t, \mathbf{x}_v) \leq V_{\mathrm{MAX}}, \quad \forall t \quad (41)$$

Furthermore, the linear inequality constraint on the arm voltage in (42) is equivalent to the required constraint defined by (41).

$$v_{\mathrm{N}}(t) - \mathbf{f}^T(t)\mathbf{x}_v \leq V_{\mathrm{MAX}}, \quad \forall t \tag{42}$$

5) MINIMUM CAPACITOR STORED ENERGY REQUIREMENT

Due to the half-bridge structure of submodules, (43) needs to hold during the operation of an MMC [8], [9].

$$Jv_C(t, \mathbf{x}_v, \mathbf{x}_i, x_{eC0}) \geq v(t, \mathbf{x}_v), \quad \forall t \tag{43}$$

It can be shown that (44) is equivalent to the desired constraint in (43).

$$e_C(t, \mathbf{x}_v, \mathbf{x}_i, x_{eC0}) \geq E_{\mathrm{MIN}}(t, \mathbf{x}_v), \quad \forall t \tag{44}$$

where

$$E_{\mathrm{MIN}}(t, \mathbf{x}_v) = \frac{C_{\mathrm{eff}}}{2} v^2(t, \mathbf{x}_v) \tag{45}$$

The definition of $E_{\mathrm{MIN}pq}(t, \mathbf{x}_v)$ for any arm is given in (106). of Note that $E_{\mathrm{MIN}}(t, \mathbf{x}_v)$ is the lower bound of $e_C(t, \mathbf{x}_v, \mathbf{x}_i, x_{eC0})$. To simplify notation, the inequality (44) can be replaced by the equivalent inequality in (46).

$$\varepsilon_C(t, \mathbf{x}_v, \mathbf{x}_i, x_{eC0}) \geq 0, \quad \forall t \tag{46}$$

where

$$\varepsilon_C(t, \mathbf{x}_v, \mathbf{x}_i, x_{eC0}) = e_C(t, \mathbf{x}_v, \mathbf{x}_i, x_{eC0}) - E_{\mathrm{MIN}}(t, \mathbf{x}_v) \tag{47}$$

The definition of $\varepsilon_{Cpq}(t, \mathbf{x}_v, \mathbf{x}_i, x_{eC0})$ for any arm is given in (110). Note that the constraint defined by (46) can be revised to include a margin by introducing a positive parameter on the right-hand side of the inequality.

6) MINIMUM INITIAL CAPACITOR ENERGY

Given the definition of x_{eC0} in (22), it is clear that

$$x_{eC0} \geq 0 \tag{48}$$

It can be shown the constraint in (48) is met upon enforcing the constraint in (46). Therefore (48) is met without explicitly including it as a constraint in the formulation of the optimisation problems.

7) HARMONIC SELECTION

The notation used in this paper considers injection of all integer harmonics from 2 to N_H into arm voltages and currents as shown in (76). Generally, MMCs are operated such that a special subsets of voltage and current harmonics, $\mathcal{V}_s \subseteq \mathcal{V}$ and $\mathcal{I}_s \subseteq \mathcal{I}$, are injected.

a: EQUALITY CONSTRAINTS

A method using equality constraints is defined to enforce the selection of harmonic numbers in $\mathcal{V}_s$ and $\mathcal{I}_s$ in the optimisation problems: Square matrices $\mathbf{B}_v$ and $\mathbf{B}_i$ can be defined such that the equality constraints defined by (49) and (50) ensure that any harmonic in $\mathbf{x}_v$ and $\mathbf{x}_i$ that is an element of $\mathcal{V}_s^c \cap \mathcal{V}$ or $\mathcal{I}_s^c \cap \mathcal{I}$, respectively, is set to zero and the desired harmonic selection is achieved. The equality constraints defined by (49) and (50) appear in the optimisation problems as required.

$$\mathbf{B}_v \mathbf{x}_v = \mathbf{0} \tag{49}$$

$$\mathbf{B}_i \mathbf{x}_i = \mathbf{0} \tag{50}$$

b: SELECTION OF VOLTAGE AND CURRENT HARMONICS

Special subsets of the injected voltages and currents defined by (6) and (7) are identified. Let $\mathbb{Z}_{++}$ be the positive integers and $N_V, N_I \in \mathbb{Z}_{++}$, $N_V, N_I \leq N_H$. Let the special subsets of $\mathcal{V}$ and $\mathcal{I}$, $\mathcal{V}_s$ and $\mathcal{I}_s$, be defined as:

$$\mathcal{V}_s \triangleq \{\mathfrak{a}_i \mid \frac{\mathfrak{a}_i}{3} \in \mathbb{Z}_{++}, \frac{\mathfrak{a}_i}{2} \notin \mathbb{Z}_{++}, i = 1, \ldots N_V\} \tag{51}$$

$$\mathcal{I}_s \triangleq \{\mathfrak{b}_i \mid \frac{\mathfrak{b}_i}{2} \in \mathbb{Z}_{++}, \frac{\mathfrak{b}_i}{3} \notin \mathbb{Z}_{++}, i = 1, \ldots N_I\} \tag{52}$$

For voltage harmonics in $\mathcal{V}_s$, the injected voltages $v_{\mathrm{IV}pq}(t)$ are *zero-sequence voltages*, which are triplen harmonics utilised since they do not appear in the line-to-line output voltages [18]. Further, for current harmonics in $\mathcal{I}_s$, which are even non-triplen harmonics, it can be shown that the sum of arm currents add to I_{dc}, that is:

$$\sum_{p \in \{a,b,c\}} i_{pq}(t, \mathbf{x}_i) = I_{dc}, \quad q \in \{u, l\} \tag{53}$$

and therefore the dc-link current, I_{dc} shown in Fig. 1 is not altered by injection of circulating currents.

For the special subsets $\mathcal{V}_s$ and $\mathcal{I}_s$, it is shown in Appendix B that $\alpha = T_0/2$. Substituting $\alpha = T_0/2$ into (16) and (27) leads to:

$$v_{pl}(t, \mathbf{x}_v) = v_{pu}(t - \frac{T_0}{2}, \mathbf{x}_v), p \in \{a, b, c\} \tag{54}$$

$$i_{pl}(t, \mathbf{x}_i) = i_{pu}(t - \frac{T_0}{2}, \mathbf{x}_i), p \in \{a, b, c\} \tag{55}$$

$$e_{Cpl}(t, \mathbf{x}_v, \mathbf{x}_i, x_{eC0}) = e_{Cpu}(t - \frac{T_0}{2}, \mathbf{x}_v, \mathbf{x}_i, x_{eC0}), p \in \{a, b, c\} \tag{56}$$

Given the result in (54) and the definition of $E_{\mathrm{MIN}pq}(t, \mathbf{x}_v)$ in (106), leads to (57).

$$E_{\mathrm{MIN}pl}(t) = E_{\mathrm{MIN}pu}(t - \frac{T_0}{2}), p \in \{a, b, c\} \tag{57}$$

The relationships in (54)-(57) are termed here as the *symmetric* properties of the circuit functions.

For voltage and current harmonics in $\mathcal{V}_s$ and $\mathcal{I}_s$, it can be shown that $e_{Cpq}(t, \mathbf{x}_v, \mathbf{x}_i, x_{eC0pq})$ is T_0-periodic if and only if (58) is satisfied.

$$\frac{I_{dc}V_{dc}}{3} + I_{1g}V_{1g} + I_{1h}V_{1h} = 0 \tag{58}$$

It can be shown that $e_{Cpq}(t, \mathbf{x}_v, \mathbf{x}_i, x_{eC0})$, $E_{\mathrm{MIN}pq}(t, \mathbf{x}_v)$ and $\varepsilon_{Cpq}(t, \mathbf{x}_v, \mathbf{x}_i, x_{eC0})$ are T_0-periodic, three-phase time-offset and symmetric. The derivation is detailed in the Appendix C, Appendix D and Appendix E.

In view of the properties established for the circuit functions in the arms, the circuit function $v_{pq}(t, \mathbf{x}_v)$, $i_{pq}(t, \mathbf{x}_i)$,

$e_{Cpq}(t, \mathbf{x}_v, \mathbf{x}_i, x_{eC0})$ and $E_{\text{MIN}pq}(t, \mathbf{x}_v)$ for any arm can be determined from the corresponding circuit functions in arm *au*. This important result implies only the circuit parameters in one arm needs to be treated in the optimisation problem. For this reason, only the *upper* arm of phase *a* is considered.

C. MODEL VALIDATION

The MMC model presented in Section II contains a number of assumptions that permits the formulation of tractable optimisation problems. It is important to check that this idealised model is a good approximation of the a real MMC system. The voltage, current and energy waveforms that are derived from the model are computed in Matlab. These waveforms are compared to those generated in an MMC experimental setting to establish the validity of the model. In this comparison, the nominal and injected voltage and current harmonics are the same in the model and three-phase MMC experimental setup. The C_{eff} used in the model is set to the value used in the experimental setup (see Table 1), that is:

$$C_{\text{eff}} = \frac{5.93\text{mF}}{8} = 0.74\text{mF} \tag{59}$$

TABLE 1. Experimental system parameters.

Parameter	Value
L_{arm}	6 mH
C_{SM}	5.93 mF
No. submodules / arm, J	8
Load resistance	10 Ω
Control frequency	5 kHz

The fundamental frequency used in the Matlab-computed model and experimental setup is 10π rad/s (5Hz) which is a typical low speed operational condition in drive applications, where injection of harmonic components is often utilised to prevent excessive capacitor voltage peaks [4]. The nominal conditions and injected voltage and current parameters are presented in Table 2.

TABLE 2. Nominal and injected harmonics voltages and currents.

Parameter	Value
I_{dc}	1.5818 A
I_{1g}, I_{1h}	-2.9 A, 0A
V_{dc}	110 V
V_{1g}, V_{1h}	60V, 0V
ω_0	10π rad/s
I_{2g}, I_{2h}	1.37 A, -0.34A
I_{4g}, I_{4h}	-0.15 A, 0.22A
I_{8g}, I_{8h}	-0.08 A, 0.03A
I_{10g}, I_{10h}	-0.02 A, -0.05A
$v_{C,ave}, Jv_{C,ave}$	13.5 V, 108 V
V_{3g}, V_{3h}	-12.95V, -0.12V
V_{9g}, V_{9h}	-1.00V, -0.12V

Experimental results were obtained using the setup described in [30], with system parameters shown in Table 1. Details of the signal processor and control structure are provided in [30]. The experimental setup controls the currents and average submodule capacitor voltage, $v_{C,ave} \triangleq \text{ave}_t[v_C(t)]$, using the current control technique presented in [26].

The arm experimental energy waveforms are presented in Fig. 3. The waveforms in Fig. 3 are periodic and three-phase time offset, thus adhering to the properties shown earlier in Section III-B7. The arm *au* experimental and model energy waveforms are shown in the top-left of Fig. 4. The superscript *mo* describes the result of the (Matlab-computed) model of the MMC discussed in this paper. The resultant model waveforms are computed for arm *au* only since the waveforms of other arms are simply time-offset with respect to arm *au*. The superscript *ex* describes the result obtained from the experimental setup. The resultant $E_{\text{MIN}}(t)$ and $e_C(t)$ align closely from the model and experimental results. Note that the model waveforms have been time-shifted to adjust for sampling offset with the experimental waveforms. There is close agreement between the *mo* and *ex* results. The small discrepancies arise from the voltage drops across the semiconductors, arm inductances and resistances that were not modelled.

The resultant arm voltages and currents for the upper arms across the three phases are presented in the right two subplots of Fig. 4. The results of the model are superimposed on these experimental results. Again, close alignment of the arm voltage and current of the modelling and experimental results occurs. As expected, voltages and currents are periodic and three-phase time-offset. The nonnegative constraint (39) ensures nonnegative arm voltages and this means that bipolar (full-bridge) converters submodules are not required in the proposed approach. Rather, unipolar (half-bridge) converters can be used to implement these optimisation results if desired. It is clear from the bottom-left of Fig. 4 that each submodule capacitor voltage in an arm is are closely balanced throughout the experiment. These preliminary results provide evidence that the modelling assumptions are acceptable.

D. PROPOSED OPTIMISATION PROBLEMS STEPS

This subsection presents the "*steps*" which form part of the two-step optimisation methods proposed in this paper.

It follows from (28) that objective function in (30) is a bilinear function of injected voltage and current harmonics, and is in general nonconvex. A drawback of nonconvex objective functions is that finding a minimum does not guarantee that it is the global minimum. A benefit of convex optimisation problems is that widely-available solving techniques can consistently find optimal values to such problems [31]. Further, the minimum of convex optimisation is the global minimum.

Two-step optimisation problems that involve subsets of the optimisation variables ($\mathbf{x}_v$, $\mathbf{x}_i$ and x_{eC0}) are proposed such that each optimisation step involves a convex optimisation problem. The optimisation problem in each step is tractable and can be solved using known methods. Four optimisation steps are proposed: LPv, QPv, LPi and QPi. Their details are discussed subsequently. As will be evident, each of the proposed optimisation steps involves either the voltage

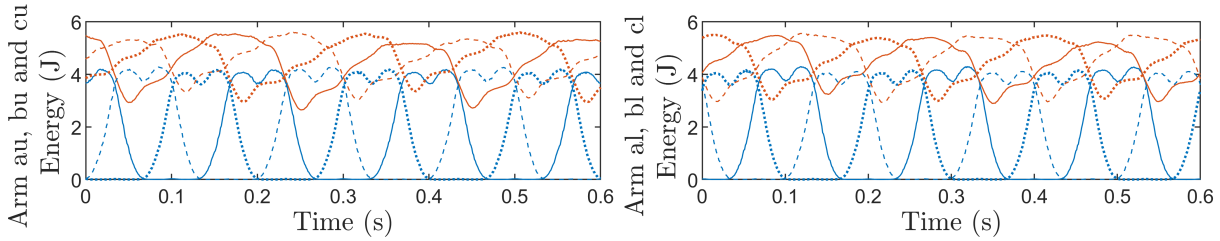

FIGURE 3. $E_{\mathrm{MIN}pq}(t)$ and $e_{Cpq}(t)$ in each upper (left) and lower (right) arm resulting from the experiment, using parameters in Tables 1 and 2. Solid lines for leg *a*, dashed lines for leg *b*, and dotted lines for leg *c*.

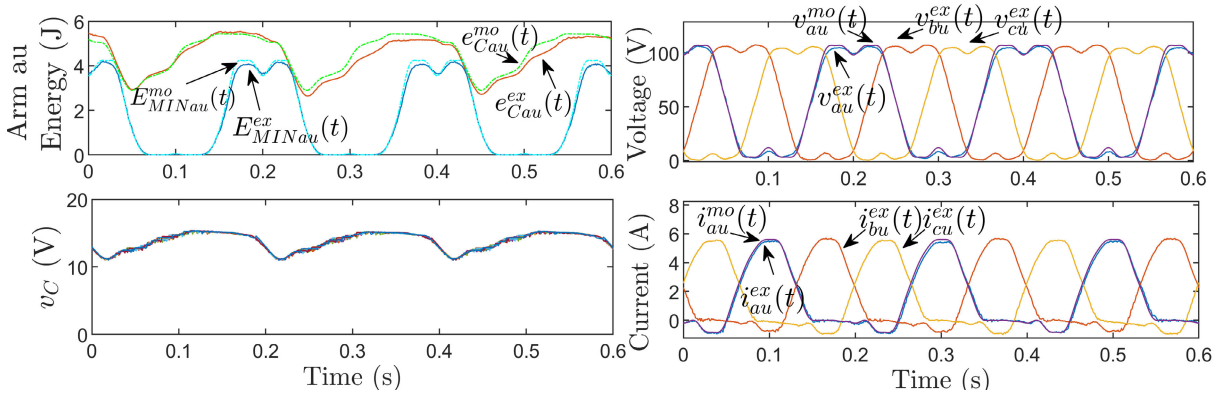

FIGURE 4. $E_{\mathrm{MIN}}(t)$ and $e_C(t)$ in arm *au* (top-left), arm voltages (top-right) and currents (bottom-right) in the upper arms, which result from Matlab-computed model, superscript *mo*, and the experimental setup, superscript *ex*. The experimental submodule capacitor voltages (bottom-left) in an arm.

parameters (LPv and QPv) or the current parameters (LPi and QPi) but not both.

All functions considered in the objective and constraints are T_0-periodic and thus every optimisation problem is solved over the interval $t \in [t_0, t_0 + T_0)$.

It is noted that if the injection of voltage harmonics is considered undesirable, then the LPv or QPv steps can be omitted, and the voltage harmonic coefficients can be set to zero.

1) QPv

QPv is the optimisation problem in (60). The optimisation problem minimizes $e_C(t, \mathbf{x}_v, \mathbf{x}_i, x_{eC0})$ over the optimisation variables $\mathbf{x}_v$ and x_{eC0} for a fixed value for $\mathbf{x}_i$ that is denoted $\bar{\mathbf{x}}_i$. From (28) it is clear that for a given $\bar{\mathbf{x}}_i$, that $e_C(t, \mathbf{x}_v, \bar{\mathbf{x}}_i, x_{eC0})$ is a linear function of $\mathbf{x}_v$ and x_{eC0}.

$$\begin{aligned} &\underset{\mathbf{x}_v, x_{eC0}}{\text{minimize}} \quad \max_{t\in[t_0,t_0+T_0)} e_C(t, \mathbf{x}_v, \bar{\mathbf{x}}_i, x_{eC0}) \\ &\text{subject to } \varepsilon_C(t, \mathbf{x}_v, \bar{\mathbf{x}}_i, x_{eC0}) \geq 0 \\ &\qquad v(t, \mathbf{x}_v) \geq 0 \\ &\qquad v(t, \mathbf{x}_v) \leq V_{\mathrm{MAX}} \\ &\qquad \mathbf{B}_v \mathbf{x}_v = \mathbf{0} \end{aligned} \tag{60}$$

From (85) it obvious that $\varepsilon_C(t, \mathbf{x}_v, \bar{\mathbf{x}}_i, x_{eC0})$ in (60) is a quadratic function of $\mathbf{x}_v$. Note that QP is an abbreviation given to the names of problems that can be formulated as a *quadratic program*.

2) LPv

Another optimisation problem step which is solved over voltage harmonics, $\mathbf{x}_v$, is proposed. An approach to reduce (30) is to minimize the maximum of $E_{\mathrm{MIN}}(t, \mathbf{x}_v)$, which is a function of only the optimisation variables, $\mathbf{x}_v$. The optimisation problem, LPv, defined by (61) is introduced.

$$\begin{aligned} &\underset{\mathbf{x}_v}{\text{minimize}} \quad \max_{t\in[t_0,t_0+T_0)} E_{\mathrm{MIN}}(t, \mathbf{x}_v) \\ &\text{subject to } v(t, \mathbf{x}_v) \geq 0 \\ &\qquad \mathbf{B}_v \mathbf{x}_v = \mathbf{0} \end{aligned} \tag{61}$$

$E_{\mathrm{MIN}}(t, \mathbf{x}_v)$ is a quadratic function of $\mathbf{x}_v$.

It can be shown that the optimisation problem in (62) is equivalent to the optimisation problem in (61) because the objective function in (62) is related to the objective function in (61) by a monotone transformation, $(\cdot)^2$, over the domain of feasible solutions [32].

$$\begin{aligned} &\underset{\mathbf{x}_v}{\text{minimize}} \quad \max_{t\in[t_0,t_0+T_0)} v(t, \mathbf{x}_v) \\ &\text{subject to } v(t, \mathbf{x}_v) \geq 0 \\ &\qquad \mathbf{B}_v \mathbf{x}_v = \mathbf{0} \end{aligned} \tag{62}$$

Note that LP is an abbreviation given to the names of problems that can be formulated as a *linear program*.

3) LPi

The optimisation problem, LPi, is defined by (63). In this problem $e_C(t, \mathbf{x}_v, \mathbf{x}_i, x_{eC0})$ is minimized with respect to the

optimisation variables $\mathbf{x}_i$ and x_{eC0} for a given $\bar{\mathbf{x}}_v$.

$$\begin{aligned}&\underset{\mathbf{x}_i, x_{eC0}}{\text{minimise}} \quad \max_{t\in[t_0,t_0+T_0)} e_C(t, \bar{\mathbf{x}}_v, \mathbf{x}_i, x_{eC0})\\ &\text{subject to } \varepsilon_C(t, \bar{\mathbf{x}}_v, \mathbf{x}_i, x_{eC0}) \geq 0\\ &\qquad |i(t, \mathbf{x}_i)| \leq I_{\text{MAX}}\\ &\qquad \mathbf{B}_v\mathbf{x}_v = \mathbf{0}\end{aligned} \tag{63}$$

4) QPi

Finally, the optimisation problem QPi is proposed. Compared to LPi the key addition in the optimisation problem QPi defined in (64) is the inclusion of a constraint on the rms current. From (37) it is clear that this is a quadratic constraint.

$$\begin{aligned}&\underset{\mathbf{x}_i, x_{eC0}}{\text{minimise}} \quad \max_{t\in[t_0,t_0+T_0)} e_C(t, \bar{\mathbf{x}}_v, \mathbf{x}_i, x_{eC0})\\ &\text{subject to } \varepsilon_C(t, \bar{\mathbf{x}}_v, \mathbf{x}_i, x_{eC0}) \geq 0\\ &\qquad |i(t, \mathbf{x}_i)| \leq I_{\text{MAX}}\\ &\qquad i^2_{rms}(t, \mathbf{x}_i) \leq (I_{\text{RMSF}} i_{rms}(\mathbf{x}_i = 0))^2\\ &\qquad \mathbf{B}_i\mathbf{x}_i = \mathbf{0}\end{aligned} \tag{64}$$

E. PROPOSED TWO-STEP OPTIMISATION PROBLEMS

The names given to each two-step optimisation problem indicates the which optimisation problems steps are solved and their sequence. For example LPvLPi solves LPv first, followed by LPi second.

The three two-step optimisation problems proposed in this paper are: 1. LPvLPi. 2. LPvQPi. 3. QPvQPi.

The selection of fixed value parameters in each step of the two-step optimisation problems are described as follows. For each two-step problem, the first step selects the fixed values to be zero, whereas the second step selects the fixed values to be the optimal values of the first step. That is, for LPv, the fixed values, $\bar{x}_{eC0}$ and $\bar{\mathbf{x}}_i$, are selected to be zero. For QPv $\bar{\mathbf{x}}_i$ is selected to be zero. For LPi and QPi, $\bar{\mathbf{x}}_v$ is selected to be the optimal $\mathbf{x}_v$ that results from LPv or QPv.

IV. OPTIMISATION IMPLEMENTATION AND RESULTS

In this section, methods are presented for the simplification, computation and comparison of the optimisation problems proposed in Section III-D.

A. DIMENSION REDUCTION

The linear equality constraints defined in (49) and (50) in each of the defined optimisation problems have a special structure which sets undesired voltage and current harmonics to zero. This structure can be exploited to reduce the dimension of the parameter vector in each of the optimisation problems. It can be shown, that there exists matrices $\mathbf{P}_{s,v}$ and $\mathbf{P}_{s,i}$ such that:

$$\mathbf{z}_v \triangleq \mathbf{P}_{s,v}\mathbf{x}_v = \begin{bmatrix} V_{\mathfrak{a}_1\, g}\\ \vdots\\ V_{\mathfrak{a}_{N_V}\, g}\\ V_{\mathfrak{a}_1\, h}\\ \vdots\\ V_{\mathfrak{a}_{N_V}\, h}\end{bmatrix}_{2N_H} \quad \mathbf{z}_i \triangleq \mathbf{P}_{s,i}\mathbf{x}_i = \begin{bmatrix} I_{\mathfrak{b}_1\, g}\\ \vdots\\ I_{\mathfrak{b}_{N_I}\, g}\\ I_{\mathfrak{b}_1\, h}\\ \vdots\\ I_{\mathfrak{b}_{N_I}\, h}\end{bmatrix}_{2N_I} \tag{65}$$

where the resulting parameter vectors of $\mathbf{z}_v$ and $\mathbf{z}_i$ contain only the injected voltages and currents of the desired sets $\mathcal{V}_s$ and $\mathcal{I}_s$, respectively. The dimensions of the vectors in (65) are reduced with respect to $\mathbf{x}_v \in \mathbb{R}^{2N_H}$ and $\mathbf{x}_i \in \mathbb{R}^{2N_H}$ in (76) because $N_V, N_I \leq N_H$. In this paper two voltage and four current harmonics are injected, $V_{3g}, V_{3h}, V_{9g}, V_{9h}$ and $I_{2g}, I_{2h}, I_{4g}, I_{4h}, I_{8g}, I_{8h}, I_{10g}, I_{10h}$, and it is found that $\mathbf{z}_v \in \mathbb{R}^4$ and $\mathbf{z}_i \in \mathbb{R}^8$.

It can be shown that the range-space of $\mathbf{P}_{s,v}$ and $\mathbf{P}_{s,i}$ is equal to the nullspace of $\mathbf{B}_v$ and $\mathbf{B}_i$, respectively. Because of this property, the equality constraints defined by matrices $\mathbf{B}_v$ and $\mathbf{B}_i$ are removed without affecting the optimal solution [31] when considering the optimisation problems in terms of the reduced dimension parameter vectors, $\mathbf{z}_v$ and $\mathbf{z}_i$.

1) PROPOSED OPTIMISATION STEPS OF REDUCED DIMENSION

Each proposed optimisation step is re-written in terms of the reduced dimension parameter vectors, $\mathbf{z}_v$ and $\mathbf{z}_i$. This reduced dimension vector form is considered hereafter and is used to generate the results in Section IV-H.

a: LPv

$$\begin{aligned}&\underset{\mathbf{z}_v}{\text{minimize}} \quad \max_{t\in[t_0,t_0+T_0)} v(t, \mathbf{z}_v)\\ &\text{subject to } v(t, \mathbf{z}_v) \geq 0\end{aligned} \tag{66}$$

b: QPv

$$\begin{aligned}&\underset{\mathbf{z}_v, x_{eC0}}{\text{minimize}} \quad \max_{t\in[t_0,t_0+T_0)} e_C(t, \mathbf{z}_v, \bar{\mathbf{z}}_i, x_{eC0})\\ &\text{subject to } \varepsilon_C(t, \mathbf{z}_v, \bar{\mathbf{z}}_i, x_{eC0}) \geq 0\\ &\qquad v(t, \mathbf{z}_v) \geq 0\\ &\qquad v(t, \mathbf{z}_v) \leq V_{\text{MAX}}\end{aligned} \tag{67}$$

c: LPi

$$\begin{aligned}&\underset{\mathbf{z}_i, x_{eC0}}{\text{minimise}} \quad \max_{t\in[t_0,t_0+T_0)} e_C(t, \bar{\mathbf{z}}_v, \mathbf{z}_i, x_{eC0})\\ &\text{subject to } \varepsilon_C(t, \bar{\mathbf{z}}_v, \mathbf{z}_i, x_{eC0}) \geq 0\\ &\qquad |i(t, \mathbf{z}_i)| \leq I_{\text{MAX}}\end{aligned} \tag{68}$$

d: QPi

$$\begin{aligned}&\underset{\mathbf{z}_i, x_{eC0}}{\text{minimise}} \quad \max_{t\in[t_0,t_0+T_0)} e_C(t, \bar{\mathbf{z}}_v, \mathbf{z}_i, x_{eC0})\\ &\text{subject to } \varepsilon_C(t, \bar{\mathbf{z}}_v, \mathbf{z}_i, x_{eC0}) \geq 0\end{aligned}$$

$$|i(t, \mathbf{z}_i)| \leq I_{\text{MAX}}$$
$$i^2_{rms}(t, \mathbf{z}_i) \leq (I_{\text{RMSF}} i_{rms}(\mathbf{z}_i = 0))^2 \quad (69)$$

B. SAMPLING

The optimisation problems defined so far involve objective functions and constraints over continuous time and hence are in general infinite dimensional problems. Discretisation of the functions in the time domain is one approach to generating finite dimensional opimization problems that approximate the infinite dimensional problems. The discretisation approach adopted in this paper is to consider uniformly sampled values over one period. The selection of appropriate sampling interval and the effect of this simple discretisation approach is an important area that requires in-depth investigation but is beyond the scope of this paper. For simplicity, the continuous time notation is retained with the understanding that t belongs to a finite set of values $\{t_0, t_0 + 1/f_s, t_0 + 2/f_s, \ldots, t_0 + T_0 - 1/f_s\}$, where f_s is the sampling frequency. As such, the optimisation problems in (66)-(69) can be solved using known numerical algorithms.

C. ALGORITHM

There exists multiple Matlab functions to solve the linear optimisation problems LPv and LPi. Examples include, *fmincon*, *fminimax* and *linprog*.

Matlab functions which can be used to solve QPv and QPi include *fmincon* and *fminimax*.

The *fmincon* Matlab function and *interior-point* algorithm [33]–[35] are selected to study the solutions of the three two-step optimisation problems. The optimisation tolerances on optimality and constraints are the same for each two-step optimisation problem considered. By using the same Matlab function and algorithm for each problem ensures the stopping criteria is consistent, which gives an effective means for comparative studies.

To solve using *fmincon*, the optimisation problems need to be transformed into the equivalent epigraph form, which is possible given the optimisation problems are convex [31]. This is achieved by introducing an auxiliary variable to the optimisation problems [31].

D. OPTIMISATION OVER A RANGE OF POWER FACTORS

The optimisation problems are solved over a range of power factors by considering the nominal operational parameters in (70).

$$\begin{aligned} V_{1g} &= -\sin(\theta_V) \quad V_{1h} = -\cos(\theta_V) \\ I_{1g} &= 0 \quad I_{1h} = 1 \end{aligned} \quad (70)$$

where $\theta_V \in [-\pi, \pi]$. Using (70), the ac components (*subscript* $\sim$) of the nominal voltages and currents are

$$v_{\text{N}\sim}(t) = \sin(\omega_0 t + \theta_V)\ \text{V} \quad (71)$$
$$i_{\text{N}\sim}(t) = \sin(\omega_0 t)\ \text{A} \quad (72)$$

Therefore, the optimisation problems can be solved over a range of power factors. Hereafter, the functions which depend on θ_V are made explicit in the arguments.

TABLE 3. Numerical optimisation parameter values.

Parameter	Value
f_0 (Hz)	50
f_s (Hz)	9000
θ_V (rad)	[-π:π/32:π]
t	[0:1/9000:1/50]
t_0	0
I_{RMSF}	[1.03:0.04:1.63]
I_{MAX} (A)	1.875
V_{MAX} (V)	244
V_{dc}, V_{1g}, V_{1h} (V)	$2, -\sin(\theta_V), -\cos(\theta_V)$
I_{dc}, I_{1g}, I_{1h} (A)	$1.5\cos(\theta_V), 0, 1$
`OptimalityTolerance`	10^{-6}
`ConstraintTolerance`	10^{-7}

E. PARAMETERS FOR NUMERICAL OPTIMISATION

The peak arm current upper bound, I_{MAX}, is selected to be:

$$I_{\text{MAX}} = 1.25 \max_{\theta_V \in [-\pi, \pi)} \left(\max_{t \in [t_0, t_0 + T_0)} (i_{\text{N}}(t, \theta_V)) \right) \quad (73)$$

The upper bound, V_{MAX}, is set to be large to keep the peak arm voltage constraint inactive and therefore exclude the effects of V_{MAX} as a factor upon comparing the different optimisation problems.

F. NOMINAL CONDITION PARAMETERS

In the nominal conditions, there are no injected voltages or currents, $\mathbf{z}_v = \mathbf{z}_i = \mathbf{0}$. The nominal parameter $x_{e_{C0}\text{N}}$ needs to be selected to satisfy the constraint in (46). In order to compare the results of the nominal conditions to those generated from the optimisation problems, a selection process is defined for the nominal $x_{e_{C0}\text{N}}$. Because the focus on this paper is on peak capacitor voltage reduction, it follows that the lowest possible $x_{e_{C0}\text{N}}$ that satisfies the condition in (46) is defined by (74).

$$x_{e_{C0}\text{N}} \triangleq \max_{t \in [t_0, t_0 + T_0)} (y(t, \theta_V)) \quad (74)$$

This is because the definition of $x_{e_{C0}\text{N}}$ in (74) implies that the minimum of the nominal ε_C, $\varepsilon_C(t, \mathbf{z}_v = \mathbf{0}, \mathbf{z}_i = \mathbf{0}, x_{e_{C0}\text{N}})$, is zero, that is:

$$\min_{t \in [t_0, t_0 + T_0)} (\varepsilon_C(t, \theta_V, \mathbf{z}_v = \mathbf{0}, \mathbf{z}_i = \mathbf{0}, x_{e_{C0}\text{N}})) = 0 \quad (75)$$

The result in (75) means that using (74) for nominal conditions creates an capacitor energy waveform which touches $E_{\text{MIN}}(t, \mathbf{z}_v = \mathbf{0})$.

G. PERFORMANCE INDICATORS

The performance indicators are defined in Table 4. Each of the performance indicators are key sources of capacitor stress [8], [9], [11] and MMC power losses [7] which are considered

to select component ratings for MMCs. Trends in these performance indicators give designers an overview of the trade-offs among power losses and stresses on components. The $\hat{}$ notation denotes a variable that is evaluated at the optimal parameters $\hat{\mathbf{z}}_v$, $\hat{\mathbf{z}}_i$ and $\hat{x}_{e_{C0}}$ that result from numerically solving the relevant two-step optimisation problems.

TABLE 4. Performance indicators.

Performance indicator	Description
$\max_t(J\hat{v}_C)$	Peak capacitor voltage
$J\hat{v}_{Crip} \triangleq \max_t J\hat{v}_C - \min_t J\hat{v}_C$	Capacitor voltage ripple
$\hat{i}_{Crip} \triangleq \max_t \hat{i}_C - \min_t \hat{i}_C$	Capacitor current ripple
$\hat{i}_{rms}$	Arm rms current
$\hat{i}_{ave} \triangleq \text{ave}_t(\lvert\hat{i}(t)\rvert)$	Arm average current

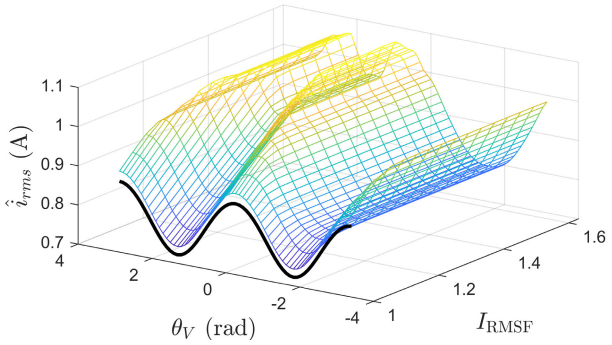

FIGURE 5. The optimal rms current at each I_{RMSF} and θ_V which results from QPvQPi using parameters in Table 3 at $C_{\text{eff}} = 3$ mF. The nominal rms current is the black line.

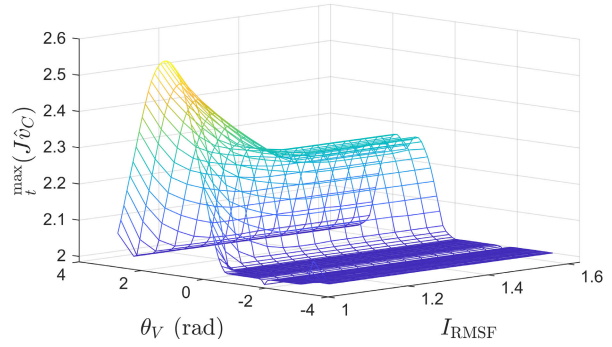

FIGURE 6. The optimal peak capacitor voltage at each I_{RMSF} and θ_V which results from QPvQPi using parameters in Table 3 at $C_{\text{eff}} = 3$ mF.

H. RESULTS COMPARISON

All three two-step optimisation problems are solved numerically for each θ_V and I_{RMSF} defined in Table 3. The resulting performance indicators for each optimisation problems at every θ_V and I_{RMSF} are termed here as the *optimisation results*.

Examples of optimisation results generated using QPvQPi are illustrated in 3D plots in Fig. 5 and Fig. 6.

Fig. 5 illustrates the rms current of QPvQPi, which approaches to the nominal rms current for all θ_V as the upper

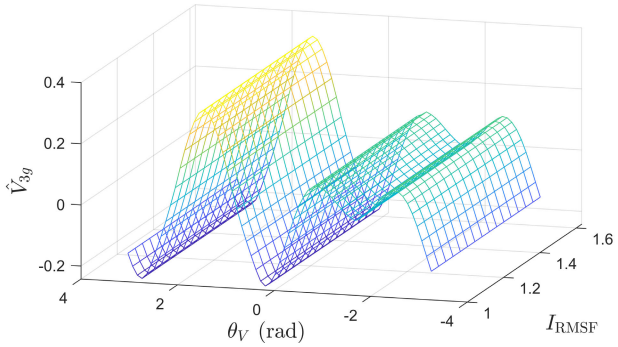

FIGURE 7. The optimal third harmonic voltage coefficient of Cosine for each I_{RMSF} and θ_V which results from QPvQPi using parameters in Table 3 at $C_{\text{eff}} = 3$ mF.

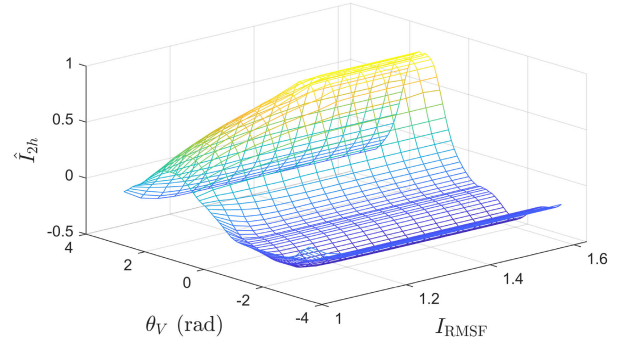

FIGURE 8. The optimal second harmonic voltage coefficient of Sine for each I_{RMSF} and θ_V which results from QPvQPi using parameters in Table 3 at $C_{\text{eff}} = 3$ mF.

bound on rms current is tightened (decreased). This is the result of defining the rms current constraint limit relative to the rms of the nominal current. It is clear from Fig. 6 that the cost incurred for reducing rms currents is the increase in peak capacitor voltages.

Examples of optimal injected voltage and current harmonic parameters, $\hat{V}_{3g} \in \hat{\mathbf{z}}_v$ and $\hat{I}_{2h} \in \hat{\mathbf{z}}_i$ are shown in Fig. 7 and Fig. 8, respectively. It is clear that as rms current constraint is loosened (increased), the optimal parameter $\hat{I}_{2h}$ increases. Together, Fig. 6 to Fig. 8 illustrate the variation of performance indicators and optimisation parameters with varying constraint, I_{RMSF}, and power factor, θ_V.

The optimisation results, which can be shown as 3D plots in Fig. 5 and Fig. 6, are condensed as 2D plots by applying the operator $\max_{\theta_V}(\cdot)$. This is for convenience of assessing overall performance in terms of the maximum, which is an important indicator for design purposes.

All 2D plots show that the LPvQPi optimisation results approach those of LPvLPi as I_{RMSF} is loosened. This occurs because the only difference between LPi and QPi is the rms current constraint. The removal of the rms current constraint from QPi, which is effectively achieved by loosening I_{RMSF}, gives the same results as LPi. LPi does not have a constraint on rms current, and therefore it is independent of I_{RMSF},

as shown by constant LPvLPi lines in the 2D plots. For the same reason, the nominal results are constant in the 2D plots.

Fig. 9 to Fig. 13 present the optimisation results for C_{eff} =3mF. Fig. 9 shows the peak capacitor voltage performance indicator as a function of I_{RMSF}. These results reflect the optimal objective criteria as the upper bound of the rms current constraint is varied. All optimisation problems give significanltly lower peak capacitor voltage compared to the nominal case. This demonstrates the effectiveness of the optimisation problems, in particular the objective function, in decreasing capacitor stress caused by peak voltage.

The peak capacitor voltage ripple, arm rms and average current, are plotted against I_{RMSF} in Fig. 10, Fig. 11 and Fig. 12, respectively. The cost of reducing arm rms current are an increase in peak capacitor voltage and peak capacitor voltage ripple. However, the benefit is a decrease in average arm current and, obviously, rms current. Lower rms and average currents give lower power losses [6], [7], [36]. These figures illustrate the trade-offs in terms of increases in the capacitor stresses and lower power losses. Further, it is clear that the I_{RMSF} is effective in limiting the rms currents which increase with circulating current injection.

The capacitor current ripple performance indicator for C_{eff} =3 mF is presented in Fig. 13. All optimisation problems result in lower capacitor current ripple with respect to the nominal, which is favourable for reducing capacitor stress. The lower capacitor stress from a combination of lower peak capacitor voltage and current ripple, along with limits on rms and average arm currents, exhibit the benefits of LPvQPi and QPvQPi. Further, QPvQPi is particularly useful when considering power losses and reducing peak capacitor voltage for all I_{RMSF}.

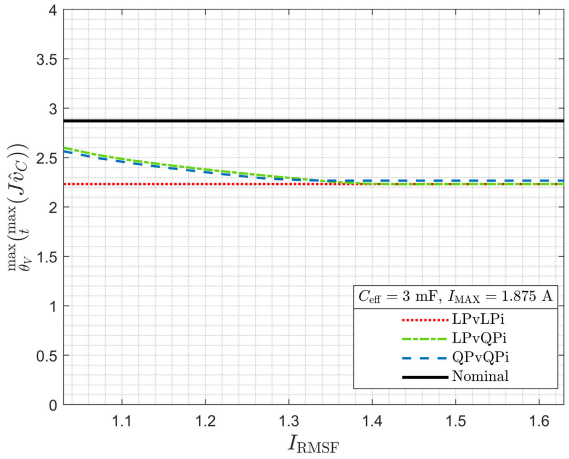

FIGURE 9. Optimal peak capacitor voltage as a function of I_{RMSF}, using parameters in Table 3 and C_{eff} = 3 mF.

The optimisation results for a larger C_{eff} (6 mF) are presented in Fig. 14 to Fig. 16. Both peak capacitor voltage and capacitor voltage ripple decrease with larger capacitance when compared to Fig. 9 and Fig. 10.

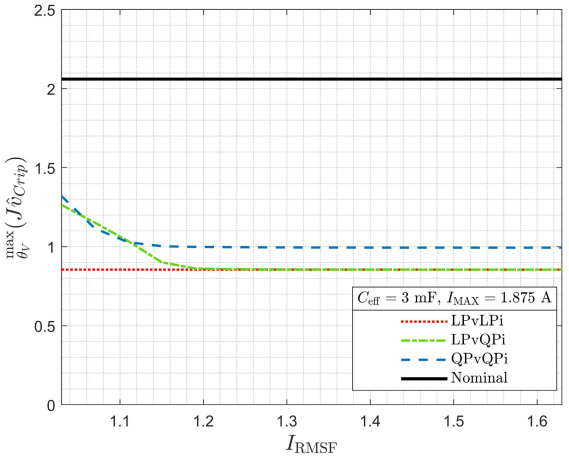

FIGURE 10. Optimal capacitor voltage ripple as a function of I_{RMSF}, using parameters in Table 3 and C_{eff} = 3 mF.

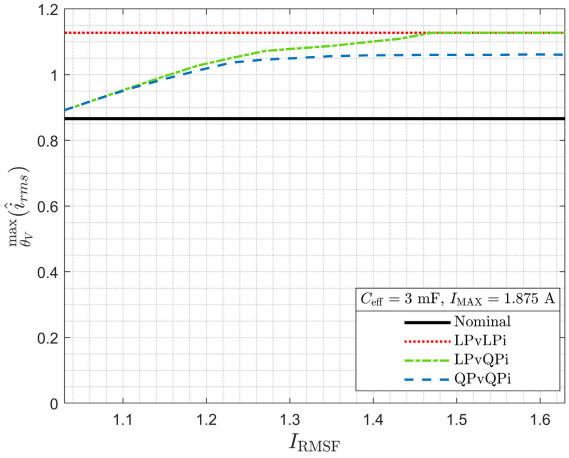

FIGURE 11. Optimal arm rms current as a function of I_{RMSF}, using parameters in Table 3 and C_{eff} = 3 mF.

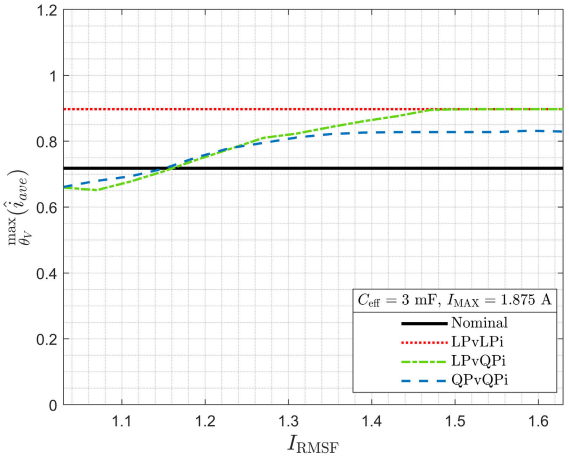

FIGURE 12. Optimal arm average current as a function of I_{RMSF}, using parameters in Table 3 and C_{eff} = 3 mF.

The capacitor current ripple is increased with respect to those presented with C_{eff} = 3mF. In addition, for C_{eff} = 6mF, the nominal capacitor current ripple is lower than those resulting from the optimisation problems.

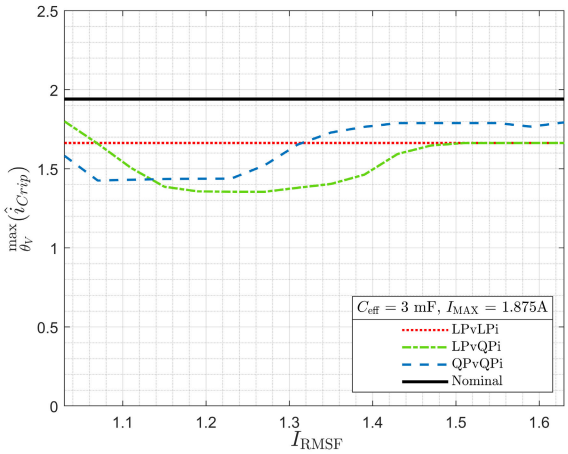

FIGURE 13. Optimal capacitor current ripple as a function of I_{RMSF}, using parameters in Table 3 and $C_{\mathrm{eff}} = 3$ mF.

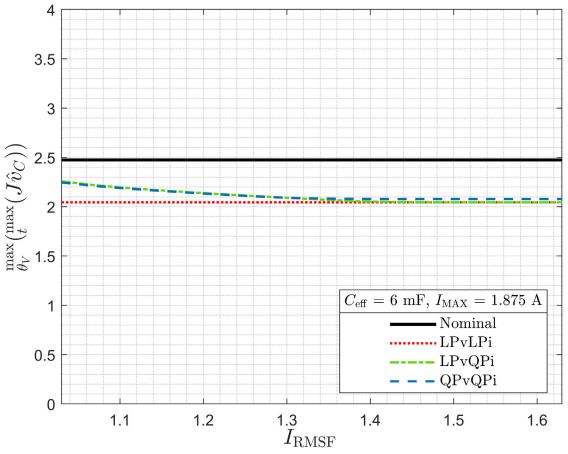

FIGURE 14. Optimal peak capacitor voltage as a function of I_{RMSF}, using parameters in Table 3 and $C_{\mathrm{eff}} = 6$ mF.

1) KEY OUTCOMES

The key outcomes of the applying the two-step optimisations are summarized as follows:

1) The peak capacitor voltages are significantly reduced with respect to the nominal for each two-step optimisation problem presented.
2) The QPi optimisation step has demonstrated its ability to constrain arm rms current and lower average current, which are important for power loss and thermal considerations.
3) For a lower capacitance value, lowering rms current does not come at a cost of capacitor voltage and current ripple that are larger than the nominal.
4) Loosening rms upper bound is beneficial in reducing capacitor stress in terms of peak and ripple capacitor voltages. However there is a trade-off since rms and average arm currents increase.
5) Holistically, LPvQPi and QPvQPi are good candidates for reducing peak capacitor voltages.

These results highlight the trade-offs which occur when optimising for lower capacitor stress and power losses. The key outcomes give designers a perspective on how the circuit parameters behave when adjusting constraints over a range of operating points.

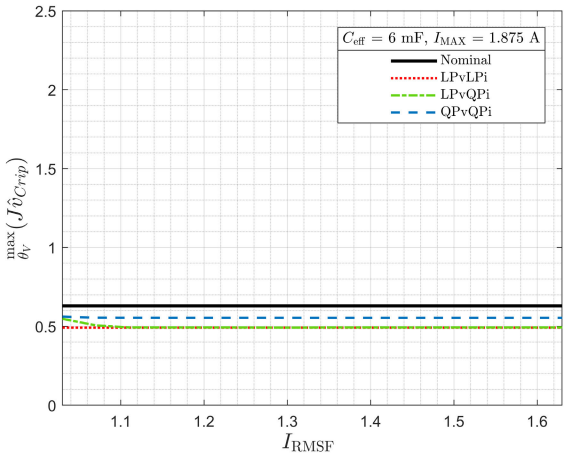

FIGURE 15. Optimal capacitor voltage ripple as a function of I_{RMSF}, using parameters in Table 3 and $C_{\mathrm{eff}} = 6$ mF.

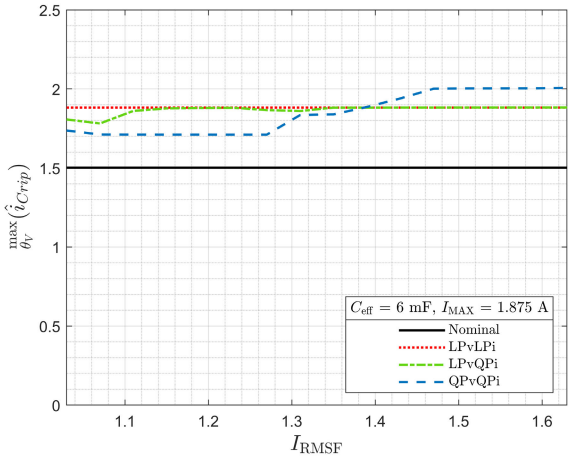

FIGURE 16. Optimal capacitor current ripple as a function of I_{RMSF}, using parameters in Table 3 and $C_{\mathrm{eff}} = 6$ mF.

V. CONCLUSION

This paper proposed three two-step convex optimisation problems which serve as tools for designers to reduce peak capacitor voltage and limiting rms currents in MMCs based on a simplified circuit model of an MMC. Each has been compared in terms of performance indicators which reflect capacitor stresses and power losses. The proposed methods have been shown to clearly identify that a trade-off that exists between capacitor stress and power losses.

Note that it is possible to consider variants of the two-step optimisation problems considered. For example, the order of QPvQPi can be changed to QPiQPv, or even alternation optimisation can be considered for the former or latter.

APPENDICES

A. VECTOR FORM OF ARM VOLTAGE AND CURRENT

The vector forms of arm voltages and currents are defined. Let the vectors containing the harmonic coefficients for voltages, $\mathbf{x}_v$, and currents, $\mathbf{x}_i$, be defined in (76). The vectors each contain coefficients for both Sine and Cosine terms for all harmonics from 2 to some integer N_H, where $N_H \geq 2$.

$$\mathbf{x}_v \triangleq \begin{bmatrix} V_{2g} \\ \vdots \\ V_{N_H g} \\ V_{2h} \\ \vdots \\ V_{N_H h} \end{bmatrix}_{2N_H}, \quad \mathbf{x}_i \triangleq \begin{bmatrix} I_{2g} \\ \vdots \\ I_{N_H g} \\ I_{2h} \\ \vdots \\ I_{N_H h} \end{bmatrix}_{2N_H} \tag{76}$$

$$\mathbf{f}_p(t) \triangleq \begin{bmatrix} \cos(2\omega_0(t-T_p)) \\ \vdots \\ \cos(N_H\omega_0(t-T_p)) \\ \sin(2\omega_0(t-T_p)) \\ \vdots \\ \sin(N_H\omega_0(t-T_p)) \end{bmatrix}_{2N_H} \tag{77}$$

1) CIRCUIT FUNCTIONS IN ARM AU

For simplicity, at times the *au* notation is dropped when considering circuit functions of the *upper* arm of leg *a*, and thus the voltage and current in arm *au* are:

$$v(t, \mathbf{x}_v) = v_{\mathrm{N}}(t) - \mathbf{f}^T(t)\mathbf{x}_v \tag{78}$$

$$i(t, \mathbf{x}_i) = i_{\mathrm{N}}(t) - \mathbf{f}^T(t)\mathbf{x}_i \tag{79}$$

where $T_p = T_q = T_{pq} = 0$ and $\mathbf{f}(t) \triangleq \mathbf{f}_a(t)$. Other key functions are defined in (80)-(83).

$$\boldsymbol{\varrho}_v(t) \triangleq \int_{t_0}^{t} \mathbf{f}(\tau) v_{\mathrm{N}}(\tau) d\tau \in \mathbb{R}^{2n}, \tag{80}$$

$$\boldsymbol{\varrho}_i(t) \triangleq \int_{t_0}^{t} \mathbf{f}(\tau) i_{\mathrm{N}}(\tau) d\tau \in \mathbb{R}^{2n}, \tag{81}$$

$$\mathbf{P}(t) \triangleq \int_{t_0}^{t} \mathbf{f}(\tau)\mathbf{f}^T(\tau) d\tau \in \mathbb{R}^{2n\times 2n}, \tag{82}$$

$$y(t) \triangleq \int_{t_0}^{t} v_{\mathrm{N}}(\tau) i_{\mathrm{N}}(\tau) d\tau - \frac{C_{\mathrm{eff}}}{2} v_{\mathrm{N}}^2(t) \tag{83}$$

Using these defined functions, it can be shown that the vector form of key circuit functions $e_C(t, \mathbf{x}_v, \mathbf{x}_i, x_{e_{C0}})$ and $\varepsilon_C(t, \mathbf{x}_v, \mathbf{x}_i, x_{e_{C0}})$ are given by (84) and (85).

$$\begin{aligned} e_C(t, \mathbf{x}_v, \mathbf{x}_i, x_{e_{C0}}) = x_{e_{C0}} &+ \int_{t_0}^{t} v_{\mathrm{N}}(\tau) i_{\mathrm{N}}(\tau) d\tau \\ &- \mathbf{x}_v^T \boldsymbol{\varrho}_i(t) - \mathbf{x}_i^T \boldsymbol{\varrho}_v(t) + \mathbf{x}_v^T \mathbf{P}(t) \mathbf{x}_i \end{aligned} \tag{84}$$

$$\begin{aligned} \varepsilon_C(t, \mathbf{x}_v, \mathbf{x}_i, x_{e_{C0}}) = y(t) + x_{e_{C0}} &- \frac{C_{\mathrm{eff}}}{2} \mathbf{x}_v^T \mathbf{f}(t)\mathbf{f}^T(t)\mathbf{x}_v \\ &+ C_{\mathrm{eff}} v_{\mathrm{N}} \mathbf{f}^T(t)\mathbf{x}_v - \boldsymbol{\varrho}_i^T(t)\mathbf{x}_v \\ &- \boldsymbol{\varrho}_v^T(t)\mathbf{x}_i + \mathbf{x}_v^T \mathbf{P}(t)\mathbf{x}_i \end{aligned} \tag{85}$$

B. VOLTAGE AND CURRENT SYMMETRY FOR $\mathcal{V}_s \subseteq \mathcal{V}$ AND $\mathcal{I}_s \subseteq \mathcal{I}$

The $T_0/2$-delayed voltage across any of the upper arms is

$$\begin{aligned} v_{pu}(t - \tfrac{T_0}{2}) = &\frac{V_{dc}}{2} \\ &- V_{1g}\cos(\omega_0(t - \tfrac{T_0}{2} - T_p)) \\ &- V_{1h}\sin(\omega_0(t - \tfrac{T_0}{2} - T_p)) \\ &- \sum_{m\in\mathcal{V}_s} V_{mg}\cos(m\omega_0(t - \tfrac{T_0}{2} - T_p)) \\ &- \sum_{m\in\mathcal{V}_s} V_{mh}\sin(m\omega_0(t - \tfrac{T_0}{2} - T_p)) \\ = &\frac{V_{dc}}{2} - V_{1g}\cos(\omega_0(t - T_p) - \pi) \\ &- V_{1h}\sin(\omega_0(t - T_p) - \pi) \\ &- \sum_{m\in\mathcal{V}_s} V_{mg}\cos(m\omega_0(t - T_p) - m\pi) \\ &- \sum_{m\in\mathcal{V}_s} V_{mh}\sin(m\omega_0(t - T_p) - m\pi) \end{aligned} \tag{86}$$

The harmonic numbers in $\mathcal{V}_s$, m, are odd, it follows that:

$$\begin{aligned} v_{pu}(t - \tfrac{T_0}{2}) = &\frac{V_{dc}}{2} \\ &+ V_{1g}\cos(\omega_0(t - T_p)) + V_{1h}\sin(\omega_0(t - T_p)) \\ &+ \sum_{m\in\mathcal{V}_s} V_{mg}\cos(m\omega_0(t - T_p)) \\ &+ \sum_{m\in\mathcal{V}_s} V_{mh}\sin(m\omega_0(t - T_p)) \\ = &\, v_{pl}(t) \end{aligned} \tag{87}$$

The $T_0/2$-delayed current in any of the upper arms is

$$\begin{aligned} i_{pu}(t - \tfrac{T_0}{2}) = &-\frac{I_{dc}}{3} \\ &+ I_{1g}\cos(\omega_0(t - \tfrac{T_0}{2} - T_p)) \\ &+ I_{1h}\sin(\omega_0(t - \tfrac{T_0}{2} - T_p)) \\ &- \sum_{m\in\mathcal{I}_s} I_{mg}\cos(m\omega_0(t - \tfrac{T_0}{2} - T_p)) \\ &- \sum_{m\in\mathcal{I}_s} I_{mh}\sin(m\omega_0(t - \tfrac{T_0}{2} - T_p)) \\ = &-\frac{I_{dc}}{3} + I_{1g}\cos(\omega_0(t - T_p) - \pi) \\ &+ I_{1h}\sin(\omega_0(t - T_p) - \pi) \\ &- \sum_{m\in\mathcal{I}_s} I_{mg}\cos(m\omega_0(t - T_p) - m\pi) \\ &- \sum_{m\in\mathcal{I}_s} I_{mh}\sin(m\omega_0(t - T_p) - m\pi) \end{aligned} \tag{88}$$

The harmonic numbers in $\mathcal{I}_s$, m, are even, it follows that

$$\begin{aligned} i_{pu}(t-\frac{T_0}{2}) = &-\frac{I_{dc}}{3} - I_{1g}\cos(\omega_0(t-T_p)) \\ &- I_{1h}\sin(\omega_0(t-T_p)) \\ &- \sum_{m\in\mathcal{I}_s} I_{mg}\cos(m\omega_0(t-T_p)) \\ &- \sum_{m\in\mathcal{I}_s} I_{mh}\sin(m\omega_0(t-T_p)) = i_{pl}(t) \end{aligned} \quad (89)$$

From (87) and (89), it is clear that $\alpha = T_0/2$.

C. PROPERTIES OF $e_{pq}(t+T_{pq}, \mathbf{x}_v, \mathbf{x}_i, x_{eC0pq})$

At times the arguments $\mathbf{x}_v$, $\mathbf{x}_i$ and x_{eC0pq} are dropped from $e_{pq}(t+T_{pq}, \mathbf{x}_v, \mathbf{x}_i, x_{eC0pq})$ to simplify notation. In this subsection, the relationship among $e_{pq}(t+T_{pq})$ for all p,q, are derived under the assumption that the time average of the $e_{pq}(t+T_{pq})$ is equal for all p,q. Consider the time-average of $e_{pq}(t+T_{pq})$:

$$\begin{aligned} &\underset{t}{\text{ave}}\, e_{pq}(t+T_{pq}) \\ &= \frac{1}{T_0}\int_{t_0}^{t_0+T_0} e_{pq}(t+T_{pq})dt \\ &= \frac{1}{T_0}\int_{t_0}^{t_0+T_0}\Bigg(\int_{t_0+T_{pq}}^{t+T_{pq}} v_{pq}(\tau,\mathbf{x}_v)i_{pq}(\tau,\mathbf{x}_i)d\tau \\ &\quad + x_{eC0pq}(t_0+T_{pq})\Bigg)dt \\ &= \frac{1}{T_0}\int_{t_0}^{t_0+T_0}\Bigg(\int_{t_0+T_{pq}}^{t+T_{pq}} v_{au}(\tau-T_{pq},\mathbf{x}_v)i_{au}(\tau-T_{pq},\mathbf{x}_i)d\tau \\ &\quad + x_{eC0pq}(t_0+T_{pq})\Bigg)dt \end{aligned} \quad (90)$$

Let $\mu = \tau - T_{pq}$, then:

$$\begin{aligned} &\underset{t}{\text{ave}}\, e_{pq}(t+T_{pq}) \\ &= \frac{1}{T_0}\int_{t_0}^{t_0+T_0}\Bigg(\int_{t_0}^{t} v_{au}(\mu,\mathbf{x}_v)i_{au}(\mu,\mathbf{x}_i)d\mu \\ &\quad + x_{eC0pq}(t_0+T_{pq})\Bigg)dt \end{aligned} \quad (91)$$

Consider now the time average energy in arm au:

$$\begin{aligned} \underset{t}{\text{ave}}\, e_{au}(t) &= \frac{1}{T_0}\int_{t_0}^{t_0+T_0} e_{au}(t)dt \\ &= \frac{1}{T_0}\int_{t_0}^{t_0+T_0}\int_{t_0}^{t} v_{au}(\tau,\mathbf{x}_v)i_{au}(\tau,\mathbf{x}_i)d\tau \\ &\quad + x_{eC0au}(t_0)dt \end{aligned} \quad (92)$$

Since it is assumed that the time-average of $e_{pq}(t+T_{pq})$ and $e_{au}(t)$ are equal, that is:

$$\underset{t}{\text{ave}}\, e_{au}(t) = \underset{t}{\text{ave}}\, e_{pq}(t+T_{pq}) \quad (93)$$

From (91), (92) and (93) it follows that:

$$x_{eC0au}(t_0) = x_{eC0pq}(t_0+T_{pq}) \quad (94)$$

Substitution of (94) in the equation for $e_{Cpq}(t+T_{pq})$ yields:

$$\begin{aligned} e_{Cpq}(t+T_{pq}) &= \int_{t_0+T_{pq}}^{t+T_{pq}} v_{pq}(\tau,\mathbf{x}_v)i_{pq}(\tau,\mathbf{x}_i)d\tau + x_{eC0au}(t_0) \\ &= \int_{t_0}^{t} v_{au}(\mu,\mathbf{x}_v)i_{au}(\mu,\mathbf{x}_i)d\tau + x_{eC0au}(t_0) \end{aligned} \quad (95)$$

Now consider the function $e_{Cau}(t)$, where $T_{pq} = T_{au} = 0$:

$$e_{Cau}(t) = \int_{t_0}^{t} v_{au}(\tau,\mathbf{x}_v)i_{au}(\tau,\mathbf{x}_i)d\tau + x_{eC0au}(t_0) \quad (96)$$

Substitution of (96) into (95) yields:

$$e_{Cpq}(t+T_{pq}) = e_{Cau}(t) \iff e_{Cpq}(t) = e_{Cau}(t-T_{pq}) \quad (97)$$

1) THREE-PHASE TIME-OFFSET

From (97), it can be shown that the relationships of $e_{Cpu}(t)$ and $e_{Cpl}(t)$ with respect to $e_{Cau}(t)$ are:

$$\begin{aligned} e_{Cpu}(t+T_p) &= e_{Cau}(t) \\ e_{Cpl}(t+T_p+\alpha) &= e_{Cau}(t) \end{aligned} \quad (98)$$

Substituting T_p into (98) for each $p \in \{a,b,c\}$, it is clear that the stored capacitor energy functions are three-phase time-offset in the upper arms as well as the lower arms.

2) SYMMETRIC PROPERTY OF $e_{Cpq}(t+T_{pq})$ FOR $\mathcal{V}_s \subseteq \mathcal{V}$ AND $\mathcal{I}_s \subseteq \mathcal{I}$

Substituting $\alpha = T_0/2$ into (98) gives (99).

$$\begin{aligned} e_{Cpu}(t+T_p) &= e_{Cau}(t) \\ e_{Cpl}(t+T_p+T_0/2) &= e_{Cau}(t) \end{aligned} \quad (99)$$

Equation (99) implies (100).

$$e_{Cpu}(t) = e_{Cpl}(t+T_0/2) \quad (100)$$

Equation (100) shows the symmetric property of $e_{Cpq}(t+T_{pq})$ for $\mathcal{V}_s \subseteq \mathcal{V}$ and $\mathcal{I}_s \subseteq \mathcal{I}$.

3) PERIODICITY FOR $\mathcal{V}_s \subseteq \mathcal{V}$ AND $\mathcal{I}_s \subseteq \mathcal{I}$

The circuit function $e_{Cpq}(t+T_{pq})$ is T_0-periodic if and only if:

$$e_{Cpq}(t+T_{pq}) = e_{Cpq}(t+T_{pq}+T_0), \forall t \quad (101)$$

Equation (101) yields:

$$\begin{aligned} &\int_{t_0+T_{pq}}^{t+T_{pq}} v_{pq}(\tau,\mathbf{x}_v)i_{pq}(\tau,\mathbf{x}_i)d\tau + x_{eC0pq}(t_0+T_{pq}) \\ &= \int_{t_0+T_{pq}}^{t+T_{pq}+T_0} v_{pq}(\tau,\mathbf{x}_v)i_{pq}(\tau,\mathbf{x}_i)d\tau + x_{eC0pq}(t_0+T_{pq}) \\ &\quad \forall t \end{aligned} \quad (102)$$

Equation (102) leads to:

$$\int_{t_0+T_{pq}}^{t+T_{pq}} v_{pq}(\tau,\mathbf{x}_v)i_{pq}(\tau,\mathbf{x}_i)d\tau$$

$$= \int_{t_0+T_{pq}}^{t+T_{pq}+T_0} v_{pq}(\tau, \mathbf{x}_v) i_{pq}(\tau, \mathbf{x}_i) d\tau, \quad \forall t \tag{103}$$

Equation (103) implies (104).

$$\int_{t+T_{pq}}^{t+T_{pq}+T_0} v_{pq}(\tau, \mathbf{x}_v) i_{pq}(\tau, \mathbf{x}_i) d\tau = 0, \quad \forall t \tag{104}$$

It can be shown that $v_{pq}(\tau, \mathbf{x}_v) i_{pq}(\tau, \mathbf{x}_i)$ contains dc components, and sinusoids with frequencies of ω_0 and integer multiples of ω_0. Therefore, (104) holds if and only if the dc component of $v_{pq}(\tau, \mathbf{x}_v) i_{pq}(\tau, \mathbf{x}_i)$ is zero. It can be shown that the dc component of $v_{pq}(\tau, \mathbf{x}_v) i_{pq}(\tau, \mathbf{x}_i)$ is equal to: $V_{dc}I_{dc}/6 + V_{1g}I_{1g}/2 + V_{1h}I_{1h}/2$, and thus $e_{Cpq}(t + T_{pq})$ is T_0-periodic if and only if:

$$\frac{V_{dc}I_{dc}}{6} + \frac{V_{1g}I_{1g}}{2} + \frac{V_{1h}I_{1h}}{2} = 0 \tag{105}$$

D. PROPERTIES OF $E_{MINpq}(t, \mathbf{x}_v)$

The definition of $E_{\mathrm{MIN}pq}(t, \mathbf{x})$ is:

$$E_{\mathrm{MIN}pq}(t, \mathbf{x}_v) \triangleq \frac{C_{\mathrm{eff}}}{2} v_{pq}^2(t, \mathbf{x}_v) \tag{106}$$

1) THREE-PHASE TIME-OFFSET

It can be shown that the relationships between $E_{\mathrm{MIN}pu}(t, \mathbf{x}_v)$ and $E_{\mathrm{MIN}pl}(t, \mathbf{x}_v)$, with respect to $E_{\mathrm{MIN}au}(t, \mathbf{x}_v)$ are given by:

$$\begin{aligned} E_{\mathrm{MIN}pu}(t + T_p, \mathbf{x}_v) &= E_{\mathrm{MIN}au}(t, \mathbf{x}_v) \\ E_{\mathrm{MIN}pl}(t + T_p + \alpha, \mathbf{x}_v) &= E_{\mathrm{MIN}au}(t, \mathbf{x}_v) \end{aligned} \tag{107}$$

Substituting T_p for each $p \in \{a, b, c\}$, it is clear that $E_{\mathrm{MIN}pq}(t, \mathbf{x}_v)$ are three-phase time-offset in the upper arms as well as the lower arms.

2) T_0-PERIODICITY

It can be shown that $E_{\mathrm{MIN}pq}(t, \mathbf{x}_v)$ can be described as a constant plus a sum of sinusoids. The greatest common frequency divisor of the sinusoids in $E_{\mathrm{MIN}pq}(t, \mathbf{x}_v)$ is the fundamental frequency, ω_0, and therefore $E_{\mathrm{MIN}pq}(t, \mathbf{x}_v)$ is T_0-periodic.

3) SYMMETRIC PROPERTY OF $E_{\mathrm{MIN}pq}$ FOR $\mathcal{V}_s \subseteq \mathcal{V}$ AND $\mathcal{I}_s \subseteq \mathcal{I}$

Substituting $\alpha = T_0/2$ into (107) gives (108).

$$\begin{aligned} E_{\mathrm{MIN}pu}(t + T_p, \mathbf{x}_v) &= E_{\mathrm{MIN}au}(t, \mathbf{x}_v) \\ E_{\mathrm{MIN}pl}(t + T_p + T_0/2, \mathbf{x}_v) &= E_{\mathrm{MIN}au}(t, \mathbf{x}_v) \end{aligned} \tag{108}$$

The equations (108) imply (109).

$$E_{\mathrm{MIN}pu}(t, \mathbf{x}_v) = E_{\mathrm{MIN}pl}(t + T_0/2, \mathbf{x}_v) \tag{109}$$

E. PROPERTIES OF $\varepsilon_{Cpq}(t, \mathbf{x}_v, \mathbf{x}_i, x_{ec0})$

At times the arguments $\mathbf{x}_v$, $\mathbf{x}_i$ and x_{ec0pq} are dropped from $\varepsilon_{Cpq}(t, \mathbf{x}_v, \mathbf{x}_i, x_{ec0pq})$ to simplify notation. The definition of $\varepsilon_{Cpq}(t)$ is given below:

$$\varepsilon_{Cpq}(t) \triangleq e_{Cpq}(t + T_{pq}) - E_{\mathrm{MIN}pq}(t, \mathbf{x}_v) \tag{110}$$

1) THREE-PHASE TIME-OFFSET

The equations in (98) and (107) imply that $\varepsilon_{Cpq}(t)$ has the following relationships:

$$\begin{aligned} \varepsilon_{Cpu}(t + T_p) &= \varepsilon_{Cau}(t) \\ \varepsilon_{Cpl}(t + T_p + \alpha) &= \varepsilon_{Cau}(t) \end{aligned} \tag{111}$$

and therefore $\varepsilon_{Cpq}(t)$ is three-phase time-offset in the upper and lower arms.

2) PERIODICITY FOR $\mathcal{V}_s \subseteq \mathcal{V}$ AND $\mathcal{I}_s \subseteq \mathcal{I}$

Under the condition in (105), and because $E_{\mathrm{MIN}pq}(t, \mathbf{x}_v)$ it T_0-periodic, it follows from (110) that $\varepsilon_{Cpq}(t)$ is T_0-periodic.

3) SYMMETRIC PROPERTY OF $\varepsilon_{Cpq}(t)$ FOR $\mathcal{V}_s \subseteq \mathcal{V}$ AND $\mathcal{I}_s \subseteq \mathcal{I}$

Substituting $\alpha = T_0/2$ into (111) gives (112).

$$\varepsilon_{Cpu}(t) = \varepsilon_{Cpl}(t + T_0/2) \tag{112}$$

F. ARM VOLTAGE, CURRENT AND ENERGY RELATIONSHIPS FOR $\mathcal{V}_s \subseteq \mathcal{V}$ AND $\mathcal{I}_s \subseteq \mathcal{I}$

The key arm voltage, current and energy relationships when considering the specific voltage and current harmonics defined for $\mathcal{V}_s$ and $\mathcal{I}_s$ are summarised below. All relationships are defined with respect to the function of arm *au*.

$$T_{pq} = T_p + \frac{T_0}{2} \tag{113}$$

$$\begin{aligned} v_{Cpq}(t) &= v_{Cau}(t - T_{pq}) \\ i_{Cpq}(t) &= i_{Cau}(t - T_{pq}) \\ E_{\mathrm{MIN}pq}(t) &= E_{\mathrm{MIN}au}(t - T_{pq}) \\ e_{Cpq}(t) &= e_{Cau}(t - T_{pq}) \\ \varepsilon_{Cpq}(t) &= \varepsilon_{Cau}(t - T_{pq}) \end{aligned} \tag{114}$$

REFERENCES

[1] M. A. Perez, S. Bernet, J. Rodriguez, S. Kouro, and R. Lizana, "Circuit topologies, modeling, control schemes, and applications of modular multilevel converters," *IEEE Trans. Power Electron.*, vol. 30, no. 1, pp. 4–17, Jan. 2015.

[2] H. Barnklau, A. Gensior, and S. Bernet, "Submodule capacitor dimensioning for modular multilevel converters," *IEEE Trans. Ind. Appl.*, vol. 50, no. 3, pp. 1915–1923, May 2014.

[3] A. Antonopoulos, L. Angquist, and H.-P. Nee, "On dynamics and voltage control of the modular multilevel converter," in *Proc. 13th Eur. Conf. Power Electron. Appl.*, 2009, pp. 1–10.

[4] S. Sau and B. G. Fernandes, "Modular multilevel converter based variable speed drive with reduced capacitor ripple voltage," *IEEE Trans. Ind. Electron.*, vol. 66, no. 5, pp. 3412–3421, May 2019.

[5] S. Debnath, J. Qin, B. Bahrani, M. Saeedifard, and P. Barbosa, "Operation, control, and applications of the modular multilevel converter: A review," *IEEE Trans. Power Electron.*, vol. 30, no. 1, pp. 37–53, Jan. 2015.

[6] K. Berringer, J. Marvin, and P. Perruchoud, "Semiconductor power losses in AC inverters," in *Proc. 13th Conf. Rec. IEEE Ind. Appl. Conf. IAS Annu. Meeting (IAS)*, vol. 1, Oct. 1995, pp. 882–888.

[7] L. Yang, Y. Li, Z. Li, P. Wang, S. Xu, and R. Gou, "A simplified analytical calculation model of average power loss for modular multilevel converter," *IEEE Trans. Ind. Electron.*, vol. 66, no. 3, pp. 2313–2322, Mar. 2019.

[8] K. Ilves, S. Norrga, L. Harnefors, and H.-P. Nee, "On energy storage requirements in modular multilevel converters," *IEEE Trans. Power Electron.*, vol. 29, no. 1, pp. 77–88, Jan. 2014.

[9] Y. Tang, L. Ran, O. Alatise, and P. Mawby, "Capacitor selection for modular multilevel converter," *IEEE Trans. Ind. Appl.*, vol. 52, no. 4, pp. 3279–3293, Jul./Aug. 2016.

[10] A. Hassanpoor, S. Norrga, H.-P. Nee, and L. Angquist, "Evaluation of different carrier-based PWM methods for modular multilevel converters for HVDC application," in *Proc. 38th Annu. Conf. IEEE Ind. Electron. Soc. (IECON)*, Oct. 2012, pp. 388–393.
[11] Y. Tang, M. Chen, and L. Ran, "A compact MMC submodule structure with reduced capacitor size using the stacked switched capacitor architecture," *IEEE Trans. Power Electron.*, vol. 31, no. 10, pp. 6920–6936, Oct. 2016.
[12] S. Engel and R. De Doncker, "Control of the modular multi-level converter for minimized cell capacitance," in *Proc. 14th Eur. Conf. Power Electron. Appl. (EPE)*, 2011, pp. 1–10.
[13] R. Picas, J. Pou, S. Ceballos, J. Zaragoza, G. Konstantinou, and V. G. Agelidis, "Optimal injection of harmonics in circulating currents of modular multilevel converters for capacitor voltage ripple minimization," in *Proc. IEEE ECCE Asia Downunder*, Jun. 2013, pp. 318–324.
[14] R. Picas, J. Pou, S. Ceballos, V. G. Agelidis, and M. Saeedifard, "Minimization of the capacitor voltage fluctuations of a modular multilevel converter by circulating current control," in *Proc. 38th Annu. Conf. IEEE Ind. Electron. Soc. (IECON)*, Oct. 2012, pp. 4985–4991.
[15] A. J. Korn, M. Winkelnkemper, and P. Steimer, "Low output frequency operation of the modular multi-level converter," in *Proc. IEEE Energy Convers. Congr. Exposit.*, Sep. 2010, pp. 3993–3997.
[16] K. Wang, Y. Li, Z. Zheng, and L. Xu, "Voltage balancing and fluctuation-suppression methods of floating capacitors in a new modular multilevel converter," *IEEE Trans. Ind. Electron.*, vol. 60, no. 5, pp. 1943–1954, May 2013.
[17] S. Debnath, J. Qin, and M. Saeedifard, "Control and stability analysis of modular multilevel converter under low-frequency operation," *IEEE Trans. Ind. Electron.*, vol. 62, no. 9, pp. 5329–5339, Sep. 2015.
[18] C. D. Townsend, G. C. Goodwin, G. Konstantinou, N. Petranovic, G. Mirzaeva, G. Farivar, and J. Pou, "Identifying circulating currents and zero-sequence voltages for reduction in stored capacitor energy in modular multilevel converters," *IEEE Trans. Ind. Electron.*, vol. 68, no. 1, pp. 454–465, Jan. 2021.
[19] C. D. Townsend, R. Aguilera, P. Acuna, G. Konstantinou, J. Pou, G. Mirzaeva, and G. C. Goodwin, "Capacitance minimization in modular multilevel converters: Using model predictive control to inject optimal circulating currents and zero-sequence voltage," in *Proc. IEEE 2nd Annu. Southern Power Electron. Conf. (SPEC)*, Dec. 2016, pp. 1–6.
[20] M. Vasiladiotis, N. Cherix, and A. Rufer, "Accurate capacitor voltage ripple estimation and current control considerations for grid-connected modular multilevel converters," *IEEE Trans. Power Electron.*, vol. 29, no. 9, pp. 4568–4579, Sep. 2014.
[21] H. R. Parikh, R. S. M. Loeches, G. Tsolaridis, R. Teodorescu, L. Mathe, and S. Chaudhary, "Capacitor voltage ripple reduction and arm energy balancing in MMC-HVDC," in *Proc. IEEE 16th Int. Conf. Environ. Electr. Eng. (EEEIC)*, Jun. 2016, pp. 1–6.
[22] K. Ilves, A. Antonopoulos, L. Harnefors, S. Norrga, L. Angquist, and H.-P. Nee, "Capacitor voltage ripple shaping in modular multilevel converters allowing for operating region extension," in *Proc. 37th Annu. Conf. IEEE Ind. Electron. Soc. (IECON)*, Nov. 2011, pp. 4403–4408.
[23] S. Ceballos, J. Pou, S. Choi, M. Saeedifard, and V. Agelidis, "Analysis of voltage balancing limits in modular multilevel converters," in *Proc. 37th Annu. Conf. IEEE Ind. Electron. Soc. (IECON)*, Nov. 2011, pp. 4397–4402.
[24] S. Mehrotra, "On the implementation of a primal-dual interior point method," *SIAM J. Optim.*, vol. 2, no. 4, pp. 575–601, 1992.
[25] Y. Zhang, "Solving large-scale linear programs by interior-point methods under the MATLAB environment," *Optim. Methods Softw.*, vol. 10, no. 1, pp. 1–31, Jan. 1998.
[26] J. Pou, S. Ceballos, G. Konstantinou, V. G. Agelidis, R. Picas, and J. Zaragoza, "Circulating current injection methods based on instantaneous information for the modular multilevel converter," *IEEE Trans. Ind. Electron.*, vol. 62, no. 2, pp. 777–788, Feb. 2015.
[27] R. Teodorescu, F. Blaabjerg, M. Liserre, and P. C. Loh, "Proportional-resonant controllers and filters for grid-connected voltage-source converters," *IEE Proc.-Electr. Power Appl.*, vol. 153, no. 5, pp. 750–762, Sep. 2006.
[28] P. Penfield, R. Spence, and S. Duinker, "A generalized form of Tellegen's theorem," *IEEE Trans. Circuit Theory*, vol. 17, no. 3, pp. 302–305, Aug. 1970.
[29] H. Barnklau, A. Gensior, and S. Bernet, "Derivation of an equivalent submodule per arm for modular multilevel converters," in *Proc. 15th Int. Power Electron. Motion Control Conf. (EPE/PEMC)*, Sep. 2012, p. LS2a-2.
[30] G. Konstantinou, S. Ceballos, I. Gabiola, J. Pou, B. Karanayil, and V. G. Agelidis, "Flexible prototype of modular multilevel converters for experimental verification of DC transmission and multiterminal systems," in *Proc. Asian Conf. Energy, Power Transp. Electrific. (ACEPT)*, Oct. 2017, pp. 1–6.
[31] S. Boyd and L. Vandenberghe, *Convex Optimization*. Cambridge, U.K.: Cambridge Univ. Press, 2004.
[32] G. C. Calafiore and L. El Ghaoui, *Optimization Models*. Cambridge, U.K.: Cambridge Univ. Press, 2014.
[33] R. H. Byrd, M. E. Hribar, and J. Nocedal, "An interior point algorithm for large-scale nonlinear programming," *SIAM J. Optim.*, vol. 9, no. 4, pp. 877–900, Jan. 1999.
[34] R. H. Byrd, R. B. Schnabel, and G. A. Shultz, "Approximate solution of the trust region problem by minimization over two-dimensional subspaces," *Math. Program.*, vol. 40, nos. 1–3, pp. 247–263, Jan. 1988.
[35] R. A. Waltz, J. L. Morales, J. Nocedal, and D. Orban, "An interior algorithm for nonlinear optimization that combines line search and trust region steps," *Math. Program.*, vol. 107, no. 3, pp. 391–408, Jul. 2006.
[36] X. Li, Q. Song, W. Liu, S. Xu, Z. Zhu, and X. Li, "Performance analysis and optimization of circulating current control for modular multilevel converter," *IEEE Trans. Ind. Electron.*, vol. 63, no. 2, pp. 716–727, Feb. 2016.

NIKOLA PETRANOVIC (Member, IEEE) received the B.Sc. and master's degrees (with Distinction) in professional engineering (electrical and electronic engineering) from The University of Western Australia, Crawley, Australia. He is currently pursuing the Ph.D. degree with The University of Western Australia. His research interests include optimization and power electronics.

ANTONIO CANTONI (Life Fellow, IEEE) was born in Soliera, Italy, in 1946. He received the B.E. (Hons.) and Ph.D. degrees from The University of Western Australia, Perth, WA, Australia, in 1968 and 1972, respectively. In 1972, he was a Lecturer in computer science with the Australian National University, ACT, Australia. In 1973, he joined the Department of Electrical and Electronic Engineering, The University of Newcastle, NSW, Australia, where he held the Chair of Computer Engineering until 1986. In 1987, he joined QPSX Communications Ltd., Perth, Australia, as the Director of the Digital and Computer Systems Design Section, where he was involved in the development of the DQDB metropolitan area network. From 1987 to 1990, he was a Visiting Professor with the Department of Electrical and Electronic Engineering, The University of Western Australia. From 1992 to 1997, he was the Director of the Western Australian Telecommunications Research Institute and a Professor of Telecommunications with the Curtin University of Technology, Bentley, WA, Australia, and the Director of the Cooperative Research Centre for Broadband Telecommunications and Networking. From 1997 to 2000, he was the Chief Technology Officer of Atmosphere Networks, an optical networks startup that he co-founded. He was the 22nd annual Alexander Graham Bell Lecturer 1999, McMaster University, ON, Canada. From 2000 to 2009, he was the Research Director of the Western Australian Telecommunications Research Institute. From 2009 to 2012, he was a Senior Research Scientist with the ICT Centre, CSIRO Australia, where he worked on the Ngara Broadband Internet Project. Since 2000, he has been a Winthrop Professor with the Department of Electrical Electronic and Computer Engineering, The University of Western Australia. His research interests include adaptive signal processing, wireless communications, electronic system design, phase-locked loops, and networking. He has received a number of awards including the 1999 Western Australia IT&T Achiever Award, the 2001 Australian Government Centenary Medal, 2009 Clunies Ross Medal, 2010 Eureka Award, and 2012 CSIRO Chairman's Medal and Research Achievement award, major contributor, Ngara Backhaul Project. He has been an Associate Editor of the IEEE TRANSACTIONS ON SIGNAL PROCESSING. He is a fellow of the Australian Academy of Technological Sciences and Engineering.

CHRISTOPHER D. TOWNSEND (Member, IEEE) received the B.E. and Ph.D. degrees in electrical engineering from the University of Newcastle, Australia, in 2009 and 2013, respectively. Subsequently, he spent three years working at ABB Corporate Research, Sweden, working on next-generation high-power converter technologies. Since then, he has held various postdoctoral research positions including at the University of New South Wales, Australia; The University of Newcastle, Australia; and Nanyang Technological University, Singapore. In 2019, he joined the Department of Electrical, Electronic and Computer Engineering, The University of Western Australia, as a Senior Lecturer. He has authored more than 60 published technical papers and has been involved in several industrial projects and educational programs in the field of power electronics. His research interests include topologies and modulation strategies for multilevel converters applied in power systems, renewable energy integration, and electric vehicle applications. He is a member of the IEEE Power Electronics and Industrial Electronics societies.

GEORGIOS KONSTANTINOU (Senior Member, IEEE) received the B.Eng. degree in electrical and computer engineering from the Aristotle University of Thessaloniki, Thessaloniki, Greece, in 2007, and the Ph.D. degree in electrical engineering from The University of New South Wales (UNSW Sydney), Australia, in 2012. From 2012 to 2015, he was a Research Associate at UNSW. He is currently a Senior Lecturer with the School of Electrical Engineering and Telecommunications, UNSW Sydney. His main research interests include multilevel converters, power electronics in HVDC, renewable energy, and energy storage applications. He is an Associate Editor for the IEEE TRANSACTIONS ON POWER ELECTRONICS, IEEE TRANSACTIONS ON INDUSTRIAL ELECTRONICS, and *IET Power Electronics*.